Cracking of High Molecular Hydrocarbons by Photo Nanocatalysis

A Thesis Submitted to the Department of Chemical Engineering, School of Chemical and Materials Engineering (SCME), NUST, Islamabad, in the partial fulfillment of the requirements for the degree of

Masters of Science (MS)

In

Energetic Materials Engineering

Submitted by

Muhammad Fahad Aziz Chishti

Registration Number: NUST201260676MSCME67612F

Supervisor Dr. Habib Nasir

Co- Supervisor Dr. Syed Abdul Moiz

School of Chemical and Materials Engineering (SCME)

National University of Sciences and Technology (NUST)

H-12 Campus Islamabad 2014

IN THE NAME OF ALLAH

THE MOST MERCIFUL

THE MOST BENEFICIENT

And We made the earth burst forth with springs and the waters met for a purpose that was preordained.

(Surah-Al-Qamar)

Thesis Submission Certificate

It is certified that the entire work in the thesis i.e "Cracking of High Molecular Hydrocarbons by Photo Nanocatalysis" has been carried out by **Mr Muhammad Fahad Aziz Chishti** and completed under my supervision in School of Chemical and Materials Engineering, National University of Sciences and Technology, H-12, Islamabad, Pakistan.

Supervisor: _____

Dr Habib Nasir

School of Chemical and Materials Engineering, NUST, Islamabad.

Submitted through

Principal/Dean: _____

School of Chemical and Materials Engineering

National University of Science and Technology

Dedication….

My

Dearest Family,

Specially my brother Saad

Abstract

This research focuses on cracking of high-molecular weight hydrocarbons to more valuable compounds using photo nanocatalysts in contrast to catalysts in bulk and by applying solar energy (under visible and UV light). Emphasis remained on chalking out difference of cracking results with catalyst in bulk and in nano size under various conditions. Therefore, samples were divided on the basis of catalysts involved, whether nano or bulk and conditions applied that is under UV light and under sunlight. Initially hydrocarbons samples were set at room temperature and by using catalysts in bulk and in nano form. Catalysts used were ZnO Nanoparticles and in bulk, MgO nanoparticles and in bulk, TiO_2 nanoparticles, nitrogen doped TiO_2 nanoparticles and in bulk. At room temperature samples were examined for various length of time that is 4, 8 and 12 hours. In other set of experiments samples were set under UV light of different wavelength that is 254 nm and 366 nm for 60 and 120 minutes using above mentioned catalysts in nano and bulk form (MgO nanoparticles and in bulk, ZnO nanoparticles and in bulk and TiO_2 nanoparticles and in bulk). Resultant products were analyzed using GCMS. After going through the obtained results we can easily conclude that nanocatalysts produce better cracking results as compared to bulk catalysts. Additionally photocatalysts that is ZnO and TiO_2 display better results as compared to MgO which has broad band gap and does not easily generate electron-hole pairs.

Acknowledgements

All Commendations to **Almighty Allah**, The Most Beneficent, The Most Merciful, Who blessed me with intellect, resoluteness and determination to accomplish this research project. All the respects to His Holy Prophet Hazrat Muhammad (PBUH), who enabled us to recognize our creator.

I wish to extend my sincere gratitude to my able supervisor Dr. Habib Nasir, for giving me an opportunity to work under his supervision and kindly providing guidance throughout the study. They have been the source of inspiration and their support, encouragement, and comments have been of greatest help. I would like to thank my dissertation committee members Dr. Abdul Qadeer Malik and Dr. Iram Mehmood for their guidance, suggestions and encouragement. I also extend my special thanks to Dr. Nisar Ahmad for helping me to accomplish my research. I would like to thank Dr. Muhammad Mujahid, and Col. Nadeem Ehsan for their support and encouragement. I also extend my gratitude to Pakistan Army in general and Pakistan Army Ordnance Corps in particular for detailing me to undergo MS (Energetic Materials Engineering) at SCME (NUST). I also applaud the nice company of my class fellows, Saleem Shah, Farrukh Khattak, Imran Yousaf and Tahir Khattak. I always cherish the happy moments spent with them. I pay my homage, sweet sensation of love and respect to my family including my father, mother, brother, sisters, my wife and sweet daughters Asma and Zainab, who prayed for my success and helped at every step of mine in every possible manner. My parents taught me the value of hard work and provided me enormous support all my life. It would not have been easy without their encouragement, cooperation and prayers.

(Fahad Aziz)

Table of Contents

List of Figures

List of Tables

List of Acronyms

BET (Brunauer-Emmett-Teller)

DTA (Differential Thermal Analysis)

FTIR (Fourier Transform Infrared Spectroscopy)

GC/MS (Gas Chromatography Mass Spectroscopy)

IPA (Isopropylalcohol)

NP (Nanoparticles)

PVP (Polyvinyl pyrollodone)

PAH (Poly Aromatic Hydrocarbons)

TA (Thermal Analysis)

TGA (Thermogravometric Analysis)

SEM (Scanning Electron Microscopy)

UV/Visible (Ultra Violet/Visible spectroscopy)

X-RD (X-Ray Diffraction)

Chapter 1: Introduction

1. This chapter encompasses the details of crude petroleum their refining and further cracking into different desired deductions. In this segment information about the oils is discussed, their past and present techniques which govern their cracking.

1.1. **Hydrocarbons Cracking**

Production of lower olefins, similar to ethylene and propylene, is a primary procedure in chemical industry for the reason that the worldwide demand for these compounds is higher than any other chemicals. These are the prime feedstock in the production of polymers, man-made fibers and most plastics [1]. Ethylene, the lightest olefinic hydrocarbon, does not occur freely in nature. It represents the largest-volume petrochemical produced in the world and has not been directly used at the end, however utilized entirely as a chemical building block in the organic chemical industry. Propylene is a byproduct in ethylene production and it is mainly used to produce polypropylene[2]. Nowadays, most of ethylene is formed by the steam cracking route. In this procedure, appropriate hydrocarbons are heated to higher temperatures, in presence of steam, to crack the molecules in low molecular alkenic products. Feedstock selection is a very important parameter – along with the capacity, pyrolysis furnace operation conditions, reactor design and strict standardization of conditions – to achieve the optimum yield of desired products. The hydrocarbon feedstocks used in ethylene pyrolysis are shown in Figure 1 and, as we can see, naphta is the most common feedstock (45%)[3].

However, the rapid development of petrochemical industry led to the lack of suitable raw materials for pyrolysis process and became necessary to search for other feedstocks, such as medium and heavy oils - kerosene, gas oil and vacuum distillate. Pyrolysis of these substances is difficult because it leads to increase coke formation and ethylene production decreases. On the other hand, this development provides the utilization of other feedstocks like hydrocarbon streams in the refineries and petrochemical companies that have little meaning and need to be recycled.

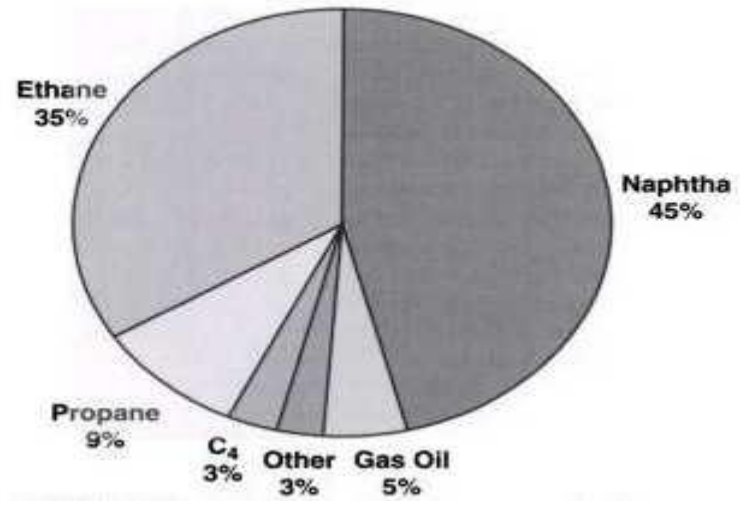

Figure 1.1 : **Worldwide feed slate percentage of ethylene production capacity [3]**

1.1.1. Thermal Cracking

The thermal decomposition of alkanes has been extensively studied since the early thirties. This led to the discovery of the reactive intermediates: the carbon free radicals and the chain reactions in organic chemistry. In the late 1940s and early 1950s kinetic – mechanistic models of a multitude of carbon free radicals and the chain reactions have been recognized. Recognized as the standard modes of hydrocarbon decompositions, helping the description of the key pyrolysis parameters and their interrelationships and consequently, allowing greater understanding of cracking furnace design and yield prediction[3, 4]. The key principles in hydrocarbon pyrolysis that can be drawn from thermodynamics and kinetics are:

- Low residence time – This is the fundamental key to greater cracking selectivity, because it can be linked to the fact that ethylene is produced primarily by first-order dissociation of larger molecules. Hence, to minimize residence time without exceeding heat flux limits, the optimal cracking coil should have a small diameter with an adequate length. The coil length-to-inside diameter ratio is an important design parameter, being the optimal value approximately 500;

- Low hydrocarbon partial pressure – Since the thermal cracking reaction results in molecular expansion, system pressure should be at minimum (Le Châtelier principle);
- High cracking conversion – Maximum ethylene yield corresponds to high conversion operation. Ethylene production pyrolysis is a high heat intensity process and the heat of cracking depends on feedstock and conversion. Consequently, conversion is a function of both residence time and temperature.

Collaterally, depending on the feed, pyrolysis also produces valuable byproducts, such as propylene, butadiene, benzene, gasoline and hydrogen. The less valuables co-products include methane and fuel oil. An important parameter in the design of commercial cracking coil is the optimal selectivity to produce the desired product slate for maximizing economic returns. The product distribution is affected by feed specifications, reactor coil, residence time, severity of operation and hydrocarbon partial pressure, as was referred to above.

1.1.2. Mechanisms of Hydrocarbon Pyrolysis

Available information on the mechanism of pyrolysis reactions are often very inconsistent and incomplete, moreover, it mostly derived from individual laboratory pyrolysis of hydrocarbons. Pyrolysis reactions of hydrocarbons can be divided in two groups – the primary and the secondary. Primary reactions comprise those leading to the first generation of pyrolysis products while the secondary include reactions involving the first generation products as educts. The hydrogen abstraction, β-scission of a C-C bond, and intramolecular isomerization are the typical examples of primary reactions. The product distribution of the primary reactions – the primary selectivity – can be used for studying the pyrolysis reactions mechanisms and with regard to the expected conversion for the industrial feedstock assessment as well [5]. It is also known that the pyrolytic reactions are very fast and strongly endothermic which require a great amount of heat delivered within the short residence time. Hydrocarbon pyrolysis reactions run mainly by radical mechanism, however, molecular reactions have also significant importance [6]. In the first phase, pyrolysis is composed mainly of intermediate influenced kinetic reactions

and in the final stage pyrolysis, on the opposite, it is controlled by the thermodynamic aspect of the process and, consequently, substances less stable, improve gradually their thermodynamic stability.

$$\bullet O_2^- + 2HO\bullet + H^+ \rightarrow H_2O_2 + O_2$$

$$HOOH \rightarrow HO\bullet + \bullet OH$$

Ultimately, the hydroxyl radicals are produced in both the reactions. These hydroxyl radicals are extremely oxidative in nature and have no selectivity with redox of (E_0 = +3.06 V).

1.2. **Nanocatalyst**

Catalytic technology is significant to present and future energy[7], chemical procedure, and ecological industries. Translation of crude oil, natural gas and coal to fuels and chemical feedstock, production of a variety of petro-chemical and chemical products, and production restrain of NO, hydrocarbons and CO all depend on catalyst used. Catalysts are vital parts of electrodes for fuel cells that employ either solid oxide ionic or polymeric proton electrolyte. Drivers for growth of superior catalysts contain (i) production of higher worth products with cheap raw materials, (ii) energy proficient and environment friendly chemical translation methods (iii) more strict ecological conventions and (iv) not expensive catalysts like with reduction or substitute of expensive metals.

In catalysis, chemical reactions in solid, gases or liquids are enhanced by incorporating a solid phase that preferably possesses large enough quantity of the precise type of spot for chemical reactants to adsorb, react, and desorbs. To gain the maximum advantage of catalyst there is need of growing numbers of sites to increase surface area, the catalytic particle size should be reduced. In modern laboratories, energetic catalysts lean to compose of cautiously arranged nanometer-range particles on supports with nanometer-sized pores or structural features. Current catalysts typically comprises of

multiple active phases that could contain a support customized to separate, isolate, or otherwise augment structure or characteristics of each catalytic particles. Primary purpose behind catalysis study is to comprehend how particle size reduction in catalyst changes its inherent catalytic efficiency further by merely increasing surface area. A consequent aim is to understand how to devise and prepare catalysts with the efficient size and structure.

1.2.1. Effect of reduction in Ctalysts Size

The thrilling prospect of nanoscience is its possible use in approximately any possible domain, ranges from medicine and electronics to manufacturing and all spheres[7]. As nano-scale technology is versatile in its application, the utility of nanocrystals as catalysts is conceivably the most fascinating. The foremost idea towards understanding nanocrystal catalysis based on the ratio of surface area and volume. With increasing the size of an object its volume increases larger in context to its surface area. Consequently, larger objects have lesser surface area with respect to their volume. This has significant inference for chemical reactions. Low volume to surface area ratios is favorable for chemical reactions. Taking campfire example, kindling is used to start the fire. The tiny pieces of wood have a greater surface area with respect to their volume than bigger logs. Therefore putting kindling on fire results in a quicker combustion. Moreover, if one throws a handful of sawdust onto a burning fire, a huge flame results. This reaction is chemically similar to normal wood burning, but it proceeds at a much faster rate. The broad function of catalysts is to augment the speed of a certain reaction. This is attained through kinetic means but it does not have any effect on chemical system in terms of thermodynamic properties. Catalyst can enhance the rate of a reaction in one of three ways; (i) by lowering the activation energy of the reaction, (ii) by acting as a facilitator and fetching the reactants together more efficiently, (iii) or generate a elevated yield of one species when two or more products are produced. Keeping in view the potential use, nano-catalysts can be used in any of the manner as mentioned. Nano-materials are more efficient than bulk catalysts based on following reasons. First, their exceptionally minute size (typically 10–80 nm) produces a great surface area-to-volume ratio. Secondly, when materials are produced on the nanoscale, the properties achieved and displayed are very

much different than their bulk form and more often not at all at macroscopic scale of same species. These both reasons are an explanation for the efficacy and versatility and of nanocatalysts.

1.3. **Photocatalysis**

The word photocatalysis is primarily a amalgamation of photochemistry and catalysis which implies a catalyst that requires light to increase the rate of a chemical reaction[8]. The main difference of photocatalytic reaction with the conventional catalytic reaction is that catalyst is activated by light rather than heat. In general, photocatalytic process can be classified as homogeneous or heterogeneous photocatalysis based on the difference in phases of catalyst and the reacting species. However heterogeneous photocatalysts is more extensively considered in present years because of prospective utilization in a number of environmental and energy associated implementation as well as in organic syntheses. In heterogeneous photo catalysis, the reaction method entails the development of an interface among a solid photocatalysts (metal or semiconductor) and a solution containing the products and reactants of the reaction. Reactions relating illuminated adsorbate-metal interface are normally studied in branch of photochemistry. Therefore the expression "heterogeneous photo catalysis" is primarily used in situations where a light absorbing semiconductor photocatalysts are used, which get in contact with phase other than solid that is either a liquid or a gas phase. At the same time heterogeneous photo catalysis can be defined as catalytic process during which one or more reaction steps occur by means of production of electron-hole pairs by suitable light on the surface of the solid semiconductor materials. The distribution and utilization of light-energy due to the occurrence of solid phase catalyst material in liquid or gaseous mixtures makes this method more multifarious as compared to homogeneous process.

1.3.1. Hetrogeneous photocatlysis

In heterogeneous photocatalysis [9], a redox reaction is mediated by a photocatalyst, which plays an important role in this reaction. As semiconductor has specific electronic arrangement of an empty conduction band and a filled valence band

and, it can be used as photocatalyst. The energy gap between the valence band and conduction band is denoted as band gap energy. Activation of a semiconductor photocatalyst could be gained by the absorption of ultra-bandgap energy photon that results in the electron-hole pair by promotion of an electron, e^-, from the valence band into the conduction band; and consequently, a hole, h^+, is produced in the valence band [10]. Sufficient lifetime is available with electron-hole pair on the excitation of semiconductor across the band gap, to undertake charge transfer to adsorbed species on the semiconductor surface from solution or gas phase contact though it is in nano-seconds regime. If the semiconductor maintains its entity, and the rate of charge transfer to the adsorbed species is uninterrupted and exothermic, the progression is termed heterogeneous photocatalysis. The number of electron-hole pairs in a semiconductor particle is reliant on the semiconductor's electronic characteristics that prevent them from recombining and the strength of the incident light. Figure 1.2 shows the phenomenon as incident light with energy equal or more than the semiconductors band gap cause excitation in electrons to move from the valance band to the conduction band. The migration of electrons and holes to the semiconductor surface results in the movement of photo-induced electron to adsorbed organic species or to the solvent. The process of electron transfer can be made more proficient if the species are pre-adsorbed on the surface [11]. Electron acceptor (usually oxygen in an aerated solution) (pathway C) can be reduced by donation of electrons by semiconductor at the surface consequently a hole may transfer to the surface where an electron from a donor species can join with the surface hole oxidizing the donor species (pathway D). The likelihood and processes of the charge transfer rate for holes and electrons rely on the redox potential levels of the adsorbate species and the relevant positions of the band edges for the valence and conduction bands. In opposition with charge movement to adsorbed species is electron and hole recombination. Recombination of the separated electron and hole can occur on the surface (pathway A) with the release of heat or in the volume of the semiconductor particle (pathway B). In classical heterogeneous photocatalytic process, the reaction itself occurs in the adsorbed phase and the overall process can be decomposed into following steps [12]:

- Transfer of reactants from the bulk of fluid to the exterior surface of the catalyst;
- Move of reactants into its pore structure from the outside surface of the catalyst;
- Adsorption of at least one of the reactants;
- Reaction in the adsorbed phase;
- Desorption of the products;
- Transport of products out of the pore structure to the exterior of the catalyst surface;
- Transport of products to the bulk of the fluid from the external surface of the catalyst.

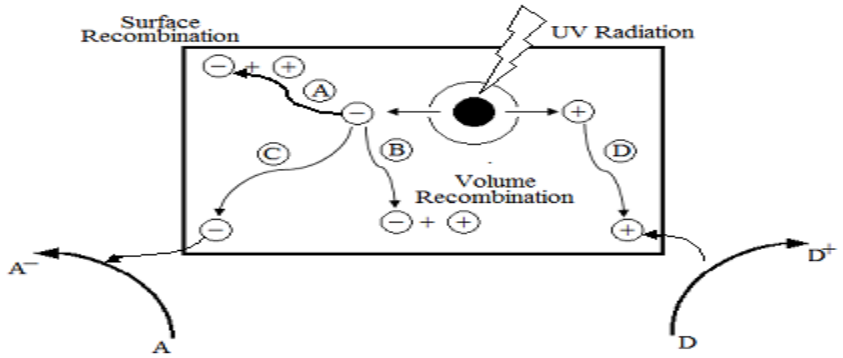

Fig 1.2: Schematic photoexcitation in a solid semiconductor

1.3.2. Mechanism involved in Photocatalysis

For a semiconductor, in order to be active as a catalyst for photocatalytic reactions, the redox potential of the photoinduced valence band hole must be sufficiently positive to generate absorbed HO radical, which can subsequently oxidize the organic pollutants, and the redox potential of the photogenerated conduction band electron must be adequately negative to be able to reduce absorbed O_2 to superoxide. In view of the utilization of energy (solar or UV light), semiconductors with lower band gap energy are more desired; however, the low bandgap semiconductors usually suffer from serious stability problems. Such semiconductors show a tendency towards photoanodic corrosion. For example, the bandgaps of p-type semiconductors are usually small, but most of them suffer serious stability problems. Therefore, p-type semiconductors are rarely used as photocatalysts. It is usually observed that an only n-type semiconductor

oxide shows stability towards photoanodic corrosion, though these semiconductors generally have so large bandgaps that they can only absorb UV light [13]. To be a good photocatalyst, some basic requirements that must be met are: 1) photoactivity; 2) ability to utilize visible and/or near UV light; 3) biological and chemical inertness; 4) photostablity; 5) low cost. Among the semiconductors, such as ZnS, ZnO, WO_3, CdS, Fe_2O_3, and TiO_2, etc., which have been investigated and reported so far, few of them are appropriate for efficient photocatalytic applications. ZnO displays unstability with respect to improper dissolution to yield $Zn(OH)_2$ on the ZnO particle surface and thus leading to inactivation of catalysts over time [14]. Although WO_3 can be activated in the visible light up to 500 nm but it is generally less photocatalytically active than TiO_2 [15]. Hematite (α-Fe_2O_3) is also absorptive in the visible range (absorption onset = 560 nm) but shows much lower photocatalytic activity than TiO_2 [16]. Although CdS has been extensively studied because of its spectral response to longer wavelength in the solar spectrum, however its usage is limited due to photo-corrosion [17]. The photocatalytic activity of ZnS has not received as much attention as TiO_2 because of its generally poor catalytic efficiency and photo-instability. As such, TiO_2 has proven to be the most suitable for widespread environmental applications [18].

1.4. **Solar Energy**

Photo catalysis has large application space to bend solar radiations which are omnipresent and abundant energy source. Renewable fuels are frequently used as easy source for energy, however their extreme use generates various serious nature problems like depletion of mineral deposits, release of green house gases and an increase in the amount of CO_2 [19]. It was therefore necessary to find an alternate of fossil fuels, which has the quality of easy availability, cheapness and no environmental hazards. And solar energy completes all above stated requirements. Solar energy is comprised of radiant (visible) light and the heat. Solar energy is the prime source of energy for all the requirements of life at our planet (Earth). Sun is the sole source of this tremendous amount of energy. Sun is composed of hydrogen, having extreme temperature which levels the ground for nuclear fusion. In hydrogen fusion two hydrogen nuclei fused in together and generate an atom of helium which results in tremendous amount of heat

release. In 2002 it was calculated that our planet (earth) including land, rivers and oceans received a total energy of almost 3,850,000 exa joules (EJ 10^{18}) per year and the amount it received in one hour was more than the energy consumed in the entire year. Solar energy we receive in one year is calculated to be twice the total energy we can ever produce from earthy minerals. It is guessed that approximately 120 million tons of hydrogen is fused to form helium in just one minute. Hence this reaction provides ground for the supply of uninterrupted solar energy which is main source of life at our planet[19].

Sun dissipates energy equally in all directions and earth receives 1400 Watts/m^2. It is assessed that sun light consists of small ultraviolet, mainly visible (400 to 700 nm) and some infrared light. There is also a very minute amount of high energy possessing x-rays which are unable to penetrate the outermost layer of atmosphere around earth because of which they are not calculated during solar energy distribution. 400 nm wave lengths are detected as violet by our eye as 600 nm is detected red. However ultra violet rays have shorter wavelength than violet and infrared posses greater than red because of which these both types of rays manage to escape from our visibility. Infrared rays are perceived as heat energy which plays an important role for temperature on earth. The graphical distribution of sun light manifests that majority of solar energy consist of visible region. Figure: 1.3 illustrates the distribution of various energy regions.

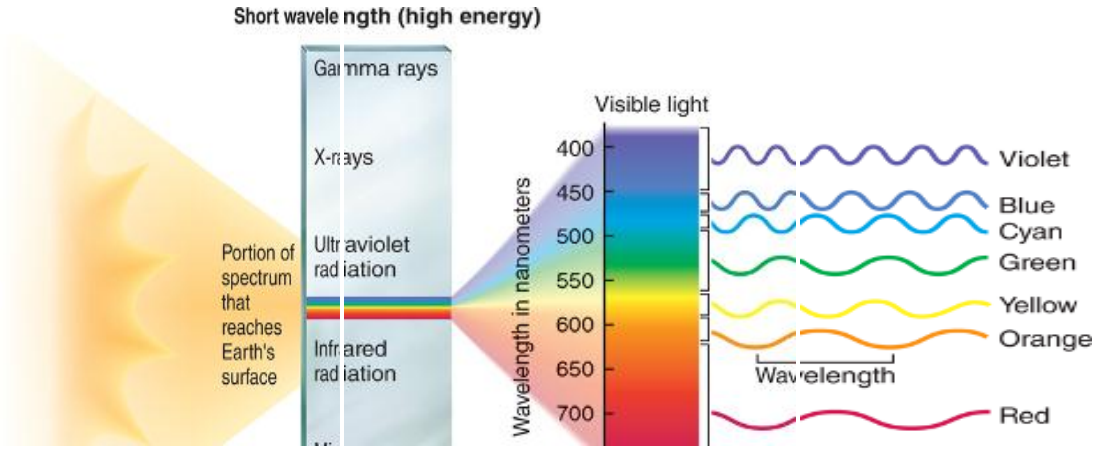

Figure 1.3: The electromagnetic spectrum, showing specifically the visible portion of Radiation

1.5. Objectives and Methodology of the Study

Objectives of the study are as under:-

1. Synthesis of Photo nano catalysts.
2. Characterization of Photo nano catalysts.
3. Chemical reaction of catalysts with hydrocarbons and analysis of products produced.
4. Further improvements in the nano catalysts.
5. Consequent improvement in hydrocarbons cracking reaction.

Methodology adopted during the project is enlisted as under:-

1. Preparation of various Photo Nanocatalysts
2. Conversion of higher molecular hydrocarbons into more useful light Olefins.
3. Devise energy efficient mechanism for higher molecular weight hydrocarbons cracking utilizing sunlight / UV light instead of thermal cracking.
4. Validating results using Analytical techniques particularly GCMS.

Chapter 2: Literature Survey

2. This chapter deals with various literature reports which define different cracking techniques used for naphtha. It is worth to highlight here that majority of petrochemical products are being produced by cracking naphtha through steam cracking at quite high temperatures. But in order to reduce the bulk of by products as well as enhance the selectivity of cracking different catalysts are being tried. It is also observed that this trend of introducing the catalysts has increased the cracking in many folds and has reduced the input of extra energy.

2.1. **Kinetic study of steam catalytic cracking (SCC) of naphtha over Fe/ZSM-5 catalyst**

In year 2012, Mehdi Sedighi et al. [20] develop a kinetic model to explain the naphtha SCC. Steam cracking of various hydrocarbons especially naphtha steam cracking is widely used to produce light olefins, ethylene and propylene at commercial scale. But, by applying only this process ever increasing worldwide requirement for light olefins cannot be satisfied, particularly of propylene. At the same time, it involves less flexibility and larger energy consumption in adjustment of product distribution. Additionally SCC is a technique of cracking hydrocarbons to light olefins in relatively low temperature with presence of a catalyst along with steam and can be considered as a potent substitute to steam cracking. SCC of diverse industrial types of hydrocarbons over ZSM-5 catalysts has been carried out. Meanwhile, naphtha is amongst the most feasible feedstock for generation of light olefins via SCC. It may also take the benefit of present facilities that are used for steam cracking. ZSM-5 zeolite has been studied extensively in various reactions such as cracking, isomerization and aromatization of hydrocarbons because of their activity, shape selectivity and larger surface area. Dissimilar element alterations have been done to enhance their selectivity to light olefins in cracking reactions.

On the basis of very deliberate studies of cracking reactions processes for naphtha SCC, a new six-lump kinetic model was formulated. The benefit of this model is to envisage ethylene and propylene directly as the major products. With only 10 anticipated kinetic parameters, good concurrence between model and experimental data was obtained. Concentration expressions of lumping species at the outlet of the reactor have been recorded. Rate constants and model parameters have been estimated with the method and experimental data. It is obvious from results as shown in figure 2.1 that a short residence time favors the production of light olefins. At the same time another important factor is reaction temperature which is directly proportional with the yield of ethylene and propylene, maximum yield of propylene ia achieved at about 680^0C with the residence time of 0.35 s and the dilution ratio of 0.5 g/g. Dilution ratio is another factor that needs to be considered as it also plays its role on production of lighter olefins.

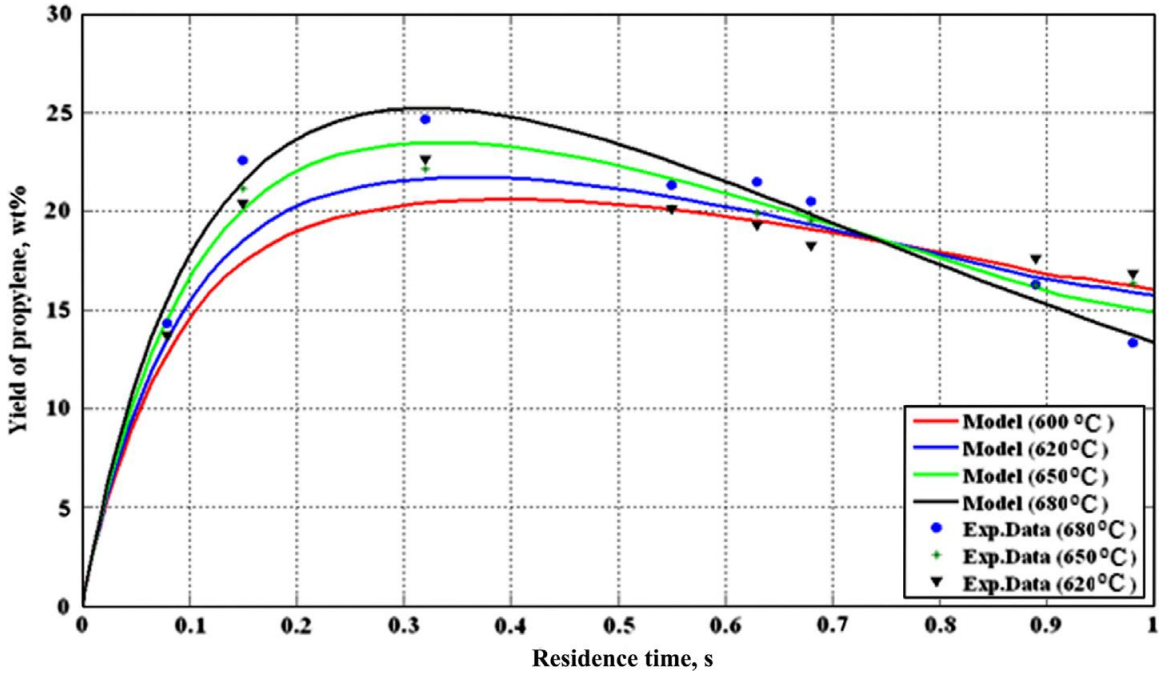

Fig. 2.1: Residence time effect on yields of propylene

2.2. **Ethylene production in naphtha thermal cracking plant in presence of steam and carbon dioxide**

In year 2013, S. Seifzadeh Haghighi et al. [21] developed a mathematical model to explain the naphtha thermal cracking. In this research work Seifzadeh Haghighi writes:

> "Thermal cracking of hydrocarbons such as naphtha, ethane, propane and their mixtures is the most common method for olefin production. Many efforts have been done on the modeling of different hydrocarbons thermal cracking. However Coke formation is a common phenomenon in thermal cracking coils that results in serious problems for pyrolysis operation. Increase in pressure drop, reduction of heat transfer and ethylene selectivity, corrosion and hot spots are the main consequences of coke deposition on walls of the cracking tubes. Among the cocking problems, heat transfer reduction has the most unfavorable effect on the process. To minimize this effect, it is vital to raise the skin temperature gradually. It is noticeable that the melting point of the building material of the furnace is a limiting factor for increasing the tube wall temperature. In addition, deposited cokes along the reactor reduce the surface area of the coils and leads to a significant pressure drop along the tubes. Typical run length of cracking furnaces is 30–90 days depending on the feed, operating conditions and the reactor types. Decoking process has to be carried out after this period of time by burning the coke using a mixture of air and steam. Unsaturated hydrocarbons and aromatics are the most important class of coke precursors due to their high reactivity and their interest for radical addition especially at high temperatures. Coke precursors are categorized into the following groups: acetylenic, olefinic, aromatics and C5+ compounds."

Advantage of this proposed model depends on the deposition of lesser quantity of coke on the interior surface of the coils as compared to conventional system which results in lesser heat buildup in tube wall. Temperature profile of the tube wall in presence of steam is far greater than the one in presence of CO_2. Clearly, less heat is moved towards the coils in presence of steam since in this case the quantity of coke formation is elevated and coke deposition act as thermal resistance. It is also obvious that the heat flux reduces in either case as the feed goes further in the furnace. Another reason for this phenomenon

to occur is the higher temperature in this part of reactor which leads to high coke thickness and same create favorable condition for coke formation.

2.3. **Catalytic cracking of naphtha to light olefins**

In year 2001, Y. Yoshimura et al. presented a catalytic process that produces light olefins from naphtha was devised to enhance the production of the conventional steam cracker. In laboratory-scale tests, a newly devised zeolite-based catalyst at a reaction temperature of 650 ◦C produced an ethylene-plus-propylene yield of about 60%, which is about 10% higher than the conventional process operated at around 820 ◦C [22].

Basic chemicals such as ethylene, propylene, and other light olefins are currently manufactured mainly from naphtha by thermal cracking, *i.e.*, so-called *steam cracking*. To cope with the requirements of higher-temperature and reduced residence time, the steam cracking process has been modified in various ways to improve energy efficiency, *e.g.*, the cracking furnace (radiant tube and coils) and heat recovery systems. However, marginal technological improvements cannot make further improvement in energy efficiency. The current steam cracking process uses as much as 40% of the energy consumed by the entire petrochemical industry. Therefore, global environmental issues have stimulated the development of processes that maximize energy and resource-savings and minimize CO_2 emissions. Besides, in the case of the current steam cracking process, it is difficult to control the composition of olefins formed. Hence, there is an increasing demand for processes capable of controlling the composition of olefins.

To respond to these needs, an association of 12 petrochemical companies which have olefin centers in Japan, have started an R&D project on naphtha catalytic cracking to replace steam cracking figure 2.2. Despite numerous patents on naphtha catalytic cracking, none of the naphtha catalytic cracking processes have been used in commercial olefin production. Nevertheless, research and development has been continued on naphtha catalytic cracking for the production of olefins, in particular ethylene, to achieve better olefin yield and lower energy consumption. In addition, uses of alternative feedstocks such as methane, LPG, gas oil, crude oil and ethanol have also been pursued.

However, the conventional naphtha is a most attractive feedstock for the petrochemical association, because it can take advantage of the existing facilities that are used for steam cracking.

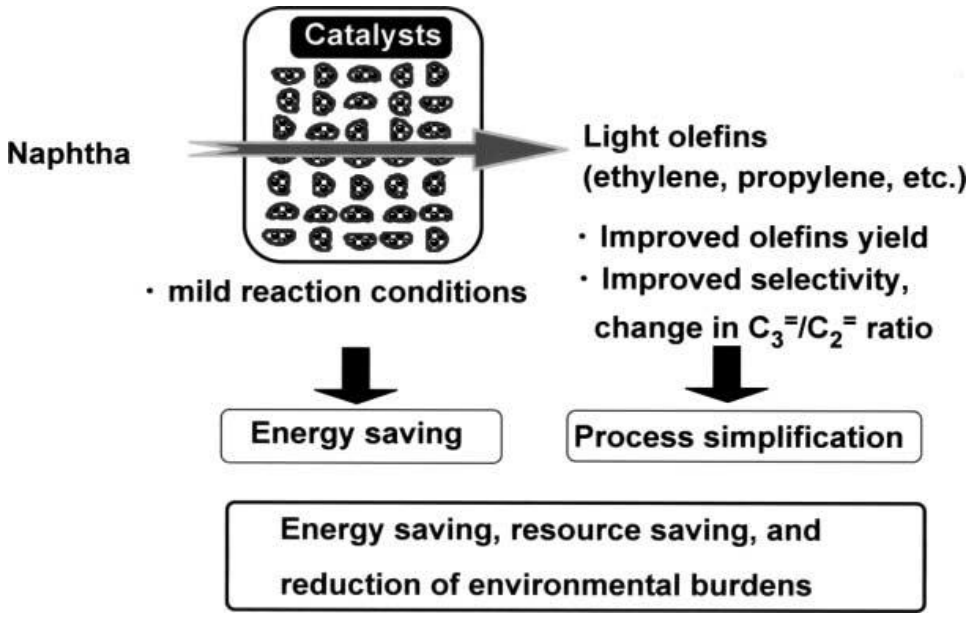

Fig. 2.2: Catalytic cracking of naphtha to light olefins.

2.4. Photocatalysts for CO_2 conversion to hydrocarbon fuels

In year 2013, Muhammad Tahir et al. presented their work on conversion of CO_2 to hydrocarbon fuels using solar energy as it appears promising to decrease global warming for enhanced sustainability. Solar energy, as direct solar irradiations, is available in very large quantum and it is advantageous to employ it for solar fuel production. This analysis paper is structured to argue recent advancements and potent applications of phototechnology to reprocess CO_2 via visible light responsive (VLR) TiO_2-based photocatalyst. In this perception different improvement processes such as doping with non-metals and metals and TiO_2 sensitization to increase its band gap toward visible region are significantly discussed [23].

Rapid global energy demand has been driven by a growing world population. Energy requirements will roughly be doubled by 2050 and tripled by the end of this

century. The current energy infrastructure is mostly dependent on fossil fuels. Greenhouse gases (GHG) particularly carbon dioxide (CO_2), the major reason of global warming is produced because of the combustion of fossil fuels. It is inevitable to explore fresh energy resources due to environment related issues, scarcity of fossil fuels and constant raise in energy requirements. Amid energy producing potentials, one method is the photochemical alteration of CO_2 into value-added chemicals. Consequently, hydrocarbons from CO_2 reduction using solar energy could be a possible source since CO_2 is green, plentiful and non-hazardous and an economical feedstock.

CO_2 reduction with H_2O through photocatalysis is very important in the growth of solar energy based carbon neutral cycle. The solar spectrum is the most abundant, permanent and reliable source of energy worth 100,000 TW; way in excess of the needs and consumptions by living things. Solar fuels include hydrogen (H_2), carbon monoxide (CO), methane (CH_4), and methanol (CH_3OH). Furthermore, CO_2 conversion to hydrocarbon fuels under solar irradiations is an economically practicable method with insignificant environmental effects.

Highly efficient and selective photocatalysts that could function under sunlight are utmost important for solar hydrocarbon production. Among the different semiconductor materials, TiO_2 as a photocatalyst has numerous advantages. Some attractive features include powerful oxidation properties, good charge transfer potentials, low cost and corrosion resistance [24]. However, TiO_2 displays activity only when irradiated with UV-light (wavelength less than 380 nm) due to its higher band gap (3.20 eV for anatase) [25]. Hence, to defeat the important restraint of UV response, different alteration techniques have been introduced in the last few years. The most frequent technique comprises doping with metals and non-metals; sensitization using dyes, nanocarbons , graphene, enzymes and novel sensitizers.

2.5. **Photocatalytic degradation of polycyclic aromatic hydrocarbons**

In year 2008, Lihong Zhang et al. presented their work on photocatalytic degradation of polycyclic aromatic hydrocarbons on soil surfaces using TiO_2 under UV

light [26]. TiO_2 is a semiconductor and because of its band gap energy it shows reponse under ultraviolet (UV) light irradiation which makes it an important candidate to be used for potential advantages in numerous cases. In the crystalline form of anatase solid TiO_2 is a semi-conductor that can promote an electron (e^-) from the valence band (VB) to the conduction band (CB) under UV irradiation creating a positive hole (h+) at the site of electron. If correct scavengers are there, oxidation/reductions may take place. Heterogeneous photocatalysis of organic pollutants using TiO_2 under UV-irradiation and/or solar light has verified successful display in a variety of remediation systems of polluted soil.

In the past few years photodegradation of PAHs in water catalyzed by TiO_2 has been studied at length. Under artificial or sunlight radiation sources TiO_2 can effectively photocatalyze the oxidation of PAHs[27]. Lihong in this paper writes:

"Phenanthrene with poor aqueous solubility was able to be easily degraded after pre-adsorbed on TiO_2 in an aqueous dispersion under UV irradiation. The pH of the dispersion and Ph/TiO_2 value had little effect on the photooxidation rate of phenanthrene catalyzed by TiO_2. In fact, PAH compounds exist as a mixture of multi-ring structures (i.e. 2-through 6-membered ring PAHs). These compounds were intentionally photocatalyzed as a mixture, more representative of the way these compounds had encountered in actual field remediation processes. Ireland et al. investigated the photocatalytic degradation of a mixture of 16 PAHs in aqueous suspensions of high surface area TiO_2 illuminated with ultraviolet light[27]. In order to enhance TiO_2 utilization rate, Garc´ıa-Mart´ınez et al. reported the photocatalytic degradation of naphthalene in water using TiO_2, supported on glass Raschig rings as catalyst. Pal and Sharon studied the photocatalytic degradation of saturated aqueous solution of naphthalene and anthracene over thin films of porous TiO_2 particles on glass substrate. However, there are few studies investigating the photocatalytic degradation of PAHs on soil surfaces using TiO_2 as the catalyst under UV irradiation".

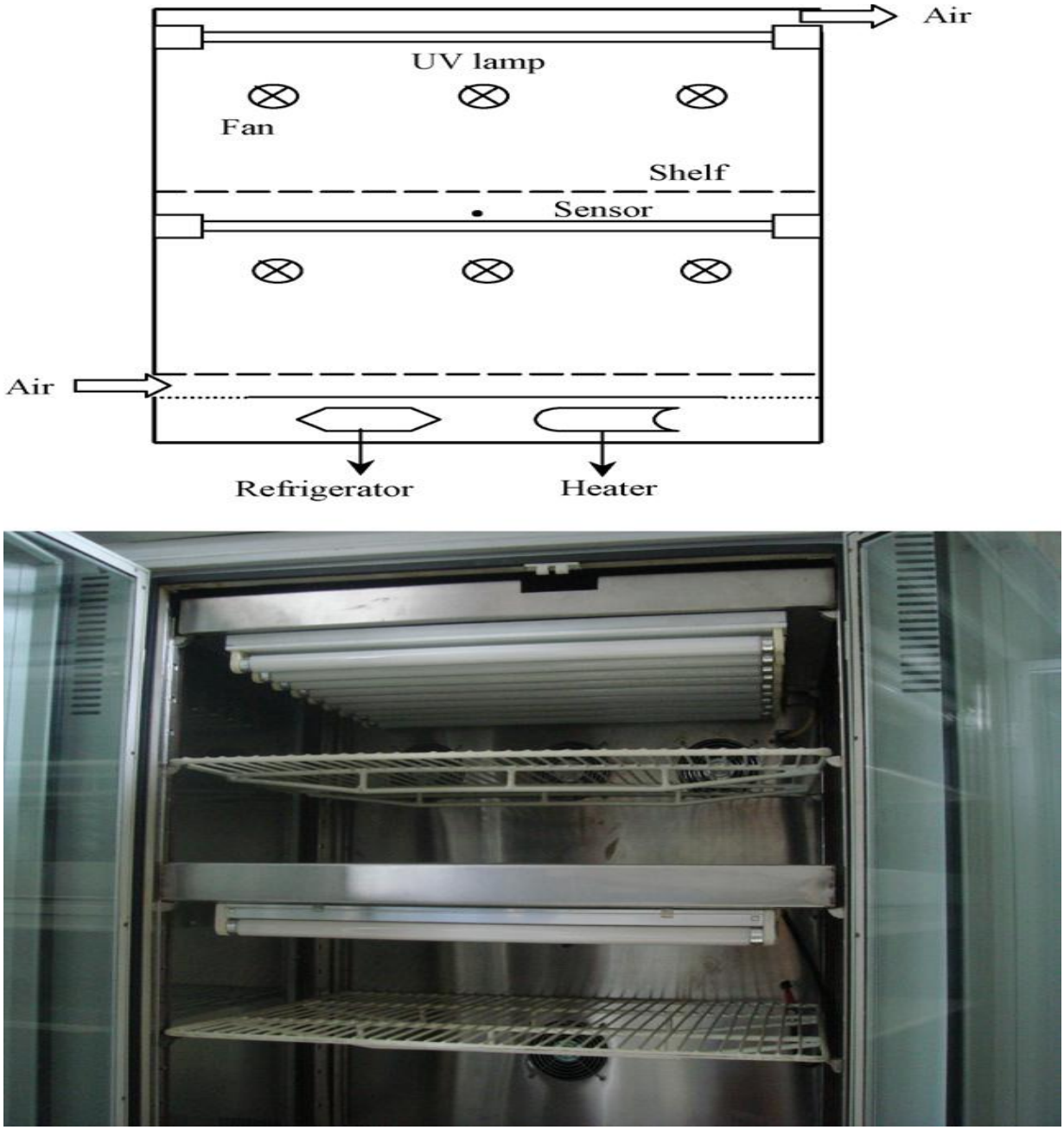

Fig. 2.3: Photodegradation Chamber for PAHs

2.6. **Synthesis and Characterization of Nanoparticles**

In year 2010, Mohammad Ali Karimi et al. proposed a sonochemical technique for synthesis of Nanoparticles of ZnO and MgO. In the recent years, lot of attention has been given to the nanostructured oxide materials and various synthesis techniques have been adopted for their production [28]. The metal oxides are enormously significant technological materials to utilize for photonic and electronic devices and also important chemical industries catalysts. These have another important application in the field of medicines as being used for production of dental cements. In last few years, scientists have researched extensively on the synthesis of nanoparticles and nanocomposite of ZnO and MgO as these have wide relevance in advanced technologies. Different physicochemical processes have been used to produce nano-sized ZnO and MgO particles. This research work aimed to adopt a novel and simple technique for production of homogeneous nano-sized ZnO and MgO particles. To achieve this, single frequency ultrasonic waves were used to avoid growth and help formation of nanoparticles. Additionally, polyvinyl pyrrolidone (PVP) was used as a structure director additive.

In year 2011, Xi-Kui Wang et al. presented a work having novel single-step synthetic method for the preparation of anatase N-doped TiO_2 nanocrystalline at low temperature [29]. Xi-Kui Wang writes:

"TiO_2 is known as one of the most effective photocatalysts for the degradation of harmful organic pollutants. However, the bandgap of TiO_2 lies in the UV range which means that only 4% of sunlight has the required energy to activate the catalyst. A visible-light activated catalyst would allow for a much larger percentage of sunlight to activate the catalyst and thus would be much more effective. Recently, extensive efforts have been made in the development of visible light driven photocatalysts that can efficiently utilize solar or indoor light [1]. As the results of these efforts, anionic dopants such as C, N, F, S and P have been introduced into the TiO_2 matrix to extend its photo response range. Among all of these anionic elements, nitrogen doping has shown greatest potential in introducing visible-light absorption because of its comparable atomic size with oxygen, small ionization energy, metastable center formation, and stability. Various methods have been used to prepare N-doped photocatalysts, including sputtering techniques, ion implantation, solvothermal process and the sol-gel method. It has also been synthesized via

sintering of TiO_2 under high temperature in a nitrogen-containing atmosphere or oxidation of titanium nitride etc. However, these processes either require a special apparatus for synthesis or require tight control of experimental conditions. Some of these methods are complicated process involve several steps, some of them have also used higher processing temperatures up to 600^oC for the incorporation of nitrogen into TiO_2. Sonochemical processing has proved to be a useful technique for generating novel materials with unusual properties. The chemical effects of sonication arise from acoustic cavitation, namely the formation, growth, and implosive collapse of bubbles in a liquid which produces unusual chemical and physical environments. The collapse of bubbles generates localized hot spots with transient temperature of about 5000 K, pressures of about 1000 atm, and cooling rates in excess of 109 K/s. Under such extreme conditions, various novel chemical reactions and physical changes occurred and numerous nano-structured materials such as metals, alloys, oxides and biomaterials had been synthesized by using high-intensive ultrasound. In this paper, we describe a novel sigle-step sonochemical method to synthesize N-doped anatase TiO_2 catalyst by use of tetraisopropyl titanate (TPT) as the titanium source and urea as the nitrogen source".

Chapter 3: Experimental Techniques

3. This chapter describes different characterization techniques used for the investigation of ultimate achieved product. Here input for these experimental equipments is also highlighted. Environment required for these techniques, their working condition along with their working principle are also mentioned too.

3.1. Particle Size Analyzer (PSA)

This experimental technique as quite obvious from its nomenclature assists to determine the particle size of sample prepared in powder form and suspended in any suitable solvent. This technique is very useful in numerous fields of industry ranging from mining to agriculture and chemistry to forestry. Particle size lying between 0.02 to 2000 microns can be examined. The particle size analyzer used at SCME, NUST is LA-920 of HORIBA Japan.

3.1.1. How PSA Works

Principle followed by PSA is laser/ light scattering. This technique is purely a physical phenomenon which reads the particle size of suspended stuff in suspension. By the help of this very technique the particle size or mean particle size of sample is determined.

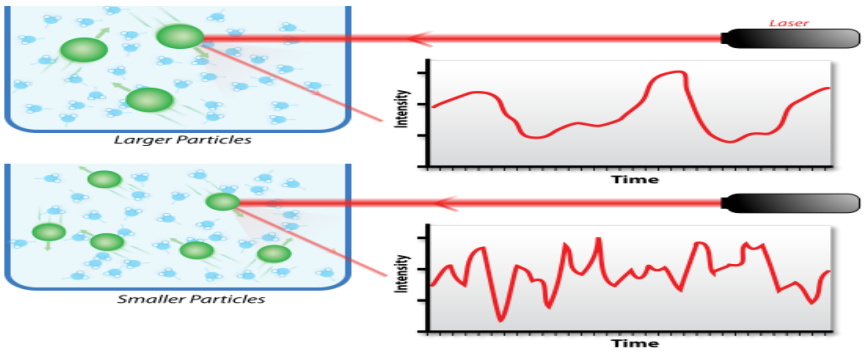

Figure 3.1: Working Principle of PSA

3.1.2. Sample Preparation

1 mg of sample was added in 500ml ethanol which was sonicated for 30 minutes. On the complete homogenous suspension of sample into ethanol 200 ml of sample was introduced into analysis chamber for its complete particle size examination.

3.2. Scanning Electron Microscope (SEM)

Scanning electron microscope (SEM) is an instrument which manifests the sample's image by a concentrated beam of electrons fired at the surface of the sample. The electron beam probes the sample surface and in retrospect an image is fabricated giving details of sample surface topography and details of its composition. The image of the sample surface comes instantly on reaching back of scattered fired electrons. The electron beam hits the atoms of the sample at the surface. SEM used here at SCME (NUST) was JSM-6490 A Analytical Scanning Electron Microscope of JEOL Japan.

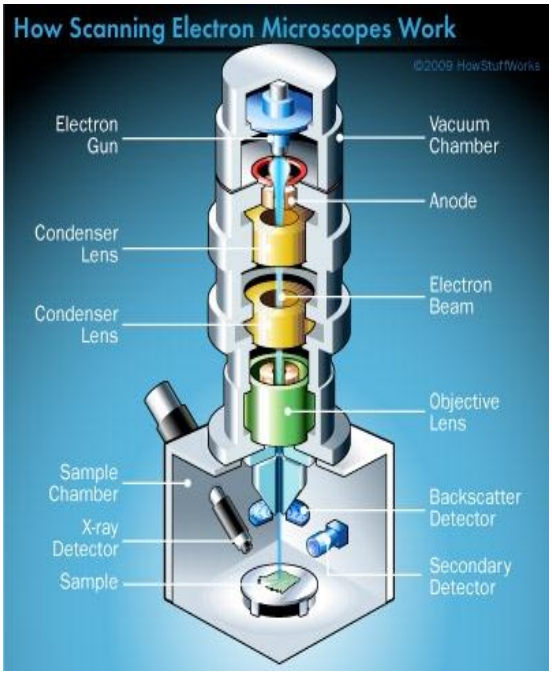

Figure 3.2: Schematic Diagram of SEM

3.2.1. SEM Working Principle

SEM generates a variety of signals from secondary electrons to back scattered ones and from transmitted electrons to x-rays. However SEM is not equipped with the detectors of each signal separately rather they all are detected by only single detector which is Secondary Electron Detector. Sample composition and its elemental form is pronounced by back scattered electrons because it is solely related to atomic number of sample. However, secondary electrons give the detailed information regarding the sample's surface and its morphology.

3.2.2. Sample Preparation

Sample preparation for the SEM varies for various sorts of samples. As for MgO, ZnO, TiO_2 and nitrogen doped TiO_2 pallets were prepared using pressing machine because a copper disc is used as carrier of sample once it is subjected to analyzing chamber of SEM. And to place the sample on the top of that copper disk of 2 mm thickness and having a diameter of 13 mm. A carbon tape adhesive is applied for holding the disc and sample together, which may give away a mixed signal once sample powder is placed on it. Therefore a pallet of required sample is made and coated with gold to make it conductive.

However, there is another technique for sample prepration i.e for MgO, ZnO and TiO_2 a very brief quantity of sample is dissolved in methanol and sonicated for 2 hours for better dispersion. Finally a drop of suspension is placed on the glass which is then subjected to analyzing chamber for detailed investigation. Said samples can even directly be placed on the carbon tape adhesive for further investigation.

3.3. X-Rays Diffraction (XRD)

XRD is a technique used to determine the crystal structure of given sample, measure spacing between inter layer or inter atomic rows and figure out the orientation of a crystal or a grain. XRD measures the internal stress of a limited crystalline regions, it

also provides information about the shape and size of a crystal. This technique is called as XRD because atomic planes present in a crystal force the X-ray beam to interfere with each other once the beam of X-ray hit the crystal region and as a result the beam diffracts on the crystals present. These are electromagnetic radiations with the wave of 10^{-10}, occupying the gap between Gamma-rays and ultra violet waves. This technique is quite helpful in sample determination vis a vis it is a non destructive technique with regard to sample analysed. This technique is being used almost in every field of science in some way or the other.

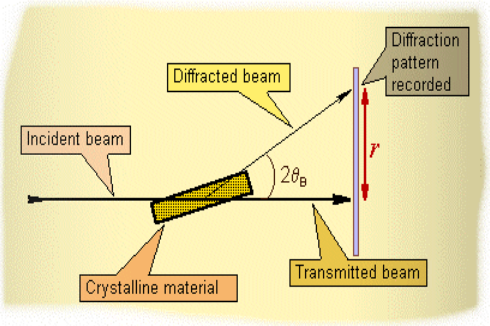

Figure 3.3: Exhibition of XRD Phenomenon

3.3.1. Working Principle of XRD

XRD works on the principle of measuring the diffraction angle after the X-rays leaves the sample, which make a certain pattern of peaks which is analyzed using Bragg's Law.

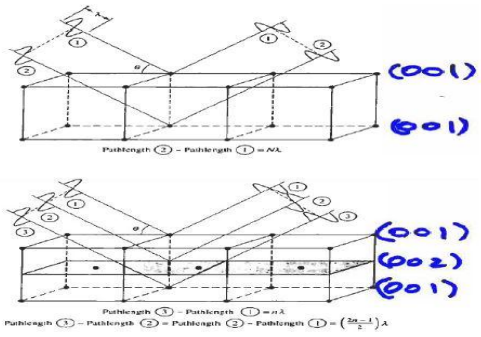

Figure 3.4: Behavior of X-ray Beam on Crystal Plane

3.4. UV-Visible Spectroscopy

Ultraviolet radiations are usually shorter in wavelength than visible and extend from 200 nm to 380 nm. UV-VIS extends from 200-800 nm, visible comes in the range from 380-800 nm and below 200 nm up to 50 nm is a vaccume ultraviolet region.

3.4.1. Basic Principle of UV-VIS Spectrophotometry

Valance shell electrons of the compound or molecule are excited from ground state to excited state when irradiated to ultraviolet or visible light. The electronic transition usually occur from highest occupied molecular orbital to lowest unoccupied molecular orbital. And the wavelength of the absorbed radiations depends mainly upon the energy difference b/w these two energy levels.

3.4.2. Working of UV-Visible Spectrophotometry

In UV-Visible spectrophotometry the light beam split into two parts, the sample beam passes through the given sample and the remaining beam passes through the reference cell containing solvent. The instrument then compares the two beams intensities. The compound will absorb light at specific wavelength and the intensity of the sample beam is less than the reference beam. The absorption spectra of pure MgO nanoparticles synthesized via different chemical routes (e.g. Sonochemical, MW assisted sonochemical and simple wet method) were recorded by using UV/Vis spectrometer (Carry-50 of SHIMADZU) in the wave length range from 200- 800 nm. All the samples in form of NPs were prepared in de-ionized water and then filtered through Whatman filter paper in order to get clear solution.

3.5. Brunauer-Emmett-Teller (BET) Method

Surface area and porosity was measured by using BET surface area and porosity analyzer (NOVA 2200e Quanta Chrome, USA). Nitrogen gas is used for adsorption and desorption. Before analyzing the samples were degassed at 300^0C for several hours. Calculated amount of sample was taken in a tube. After degassing the sample was placed

in the sample tube in sample holders then first helium gas in order to inert the atmosphere and finally passed N_2 gas for adsorption.

3.6. **Gas Chromatography–Mass Spectrometry (GCMS)**

This analytical technique is used to examine the test sample may it be gas or liquid by using chromatography or by using the mass spectrometry in order to identify the constituents of the sample. GC-MS is a helpful investigating tool used at various corridors by probing agencies for the detection of explosives, drugs, chemicals and for environmental analysis.

GCMS comprises of two components 1st gas chromatograph and 2nd mass spectrometer. GC mainly functions around capillary column, its different dimensions (diameter and length etc) and the phase properties. The interaction of two (mobile and stationary) phase will determine the separation quality, higher the retention time of mobile phase on stationary phase higher the separation of molecules and vice versa. When elute comes out of the stationary phase it is identified basing on its mass by mass spectrometer. Mass spectrometer breaks the molecule in ionized form and detects these ions on the base of mass to charge ratio. Both the detecting facilities (gas chromatograph and mass spectrometer) strengthen the detection because only single facility cannot do enough in detection of sample. Gas chromatograph (uses flame ionization detector) cannot detect the sample if ample of the molecules come together for the identification after passing through the column as they are having the same retention time. However, mass spectrometer requires a pure sample. It is almost impossible that both characteristics: cracking and retention time are same for two different molecules. So this fusion of mass spectrometer and gas chromatograph make a fine detection which is highly accurate.

GCMS used in this research is of SHIMADZU (Japan) GCMS QP 2010 ULTRA.

Figure 3.5: GCMS Display

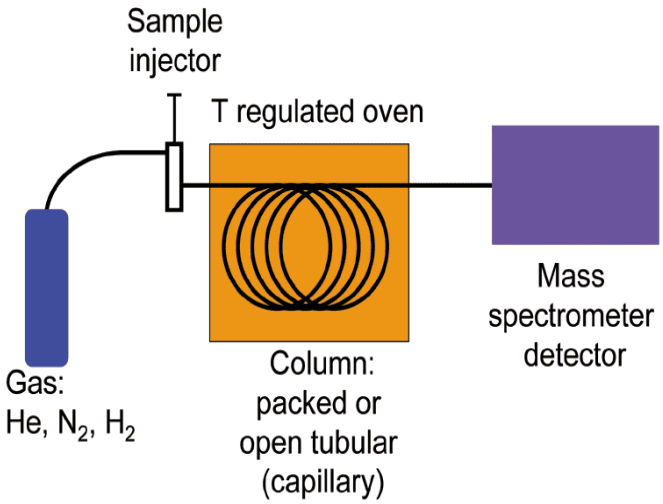

Figure 3.6: GCMS Functional Skeleton

Chapter 4: Experimental Work

4. This chapter will deal to the synthesis and characterization of different metal oxides and the description of various experimental procedures. This chapter will also present details for the different experimental setup and materials used during the experimental work. Results so obtained will be shown by graphical method and will be discussed in detail in next chapter.

4.1. Materials

$Mg(CH_3COO)_2.4H_2O$, pure (AppliChem), $Zn(CH_3COO)_2.2H_2O$, pure (Sigma Aldrich) NH_4OH (Fisher Scientific), Polyvinylpyrolidone (PVP) of Sigma Aldrich, , Ethanol (Sigma Aldrich), Titanium Tetraisopropoxide (Daejung), 2-Propanol (Sigma Aldrich) , Urea (Sigma Aldrich) .

Table 4.1: Materials Used in Different Experimental Work

Chemicals	**Purity %**	**Remarks**
$Zn(CH_3COO)_{2.}\,2H_2O$	>99%	Sigma Aldrich
$Mg(CH_3COO)_{2.}\,4H_2O$	>99%	AppliChem
NH_4OH	>99%	Fisher Scientific
PVP	>99%	Sigma Aldrich
Titanium Isopropoxide	>99%	Daejung
2-Propanol		Sigma Aldrich
Urea		Sigma Aldrich

4.2. Synthesis of Photonano Catalysts

4.2.1. Experimental Procedure for the Synthesis of MgO Nanoparticles by Sonochemical Method

The precursors used in sonochemical process for the synthesis of MgO nanoparticles were magnesium acetate tetrahydrate $Mg(CH_3COO)_2.4H_2O$, pure (AppliChem), NH_4OH (E.Merck) was used as a precipitant as well as for homogeneity and pH value of the solution, Polyvinylpyrolidone (PVP) of Sigma Aldrich was used as structure stabilizers to control morphology and size of particles [28, 30]. Atmosphere conditions were applied to perform all the experiments. First, 100 mL magnesium acetate solution (0.14M) including PVP (10 gL^{-1}) as structure director additive was sonicated for 30 min and then, sufficient amount of NH_4OH solution (0.34 M) was gradually added. In this step, nano-structured magnesium hydroxide was produced as per following reaction:

$$Mg(CH_3COO)_{2(aq)} + 2NH_4OH_{(aq)} \longrightarrow Mg(OH)_{2(s)} + 2CH_3COONH_{4\,(aq)}$$

After completion of NH_4OH solution addition in the mixture, it was sonicated for another 30 min. The magnesium hydroxide which was received in precipitate form over filter paper was washed with ethanol and distilled water for five times. Than obtained precipitate of $Mg(OH)_{2(s)}$ were mixed with 50 mL ethanol and the mixture was sonicated for 30 min and then filtered the sonicated mixture. Dehydration of the finally obtained precipitate was carried out at 550 ºC for 5 h. The subsequent reaction which took place during the dehydration phase is as under:

$$Mg(OH)_{2(s)} \longrightarrow MgO_{(s)} + H_2O_{(g)}$$

To eradicate agglomeration MgO nanoparticles were sonicated in ethanol for additional 30 min. At the last, the mixture was filtered and dried in oven at 110 ºC. The final product was obtained in nanopowder form. Characterization of nanostructured magnesium oxide powder was carried out using different techniques particularly by SEM, XRD, and UV/ Vis spectroscopy.

4.2.2. Experimental Procedure for the Synthesis of ZnO Nanoparticles by Sonochemical Method

The precursors used in sonochemical process for the synthesis of ZnO nanoparticles were zinc acetate dihydrate $Zn(CH_3COO)_2.2H_2O$, pure (Sigma Aldrich), NH_4OH (E.Merck) was used as a precipitant as well as for homogeneity and pH value of the solution, Polyvinylpyrolidone (PVP) of Sigma Aldrich was used as structure stabilizer to control morphology and size of particles [28]. Atmosphere conditions were applied to perform all the experiments. First, 100 ml zinc acetate solution (0.1M) including PVP (10 gL^{-1}) as structure director additive was sonicated for 30 min and then, sufficient amount of NH_4OH solution (0.28 M) was gradually added. In this step, nano-structured magnesium hydroxide was produced as per following reaction:

$$Zn(CH_3COO)_2\ (aq) + 2NH_4OH(aq) \longrightarrow Zn(OH)_2\ (s) + 2CH_3COONH_4\ (aq)$$

After completion of NH_4OH solution addition in the mixture, it was sonicated for another 30 min. The zinc hydroxide which was received in precipitate form over filter paper was washed with ethanol and distilled water for five times. Than obtained precipitate of $Zn(OH)_{2(s)}$ were mixed with 50 mL ethanol and the mixture was sonicated for 30 min and then filtered the sonicated mixture. Dehydration of the finally obtained precipitates was carried out at 320 ºC for 3 h. The subsequent reaction which took place during the dehydration phase is as under:

$$Zn(OH)_{2(s)} \longrightarrow ZnO_{(s)} + H_2O_{(g)}$$

To eradicate agglomeration ZnO nanoparticles were sonicated in ethanol for additional 30 min. At the last, the mixture was filtered and dried in oven at 110 ºC. The final product was obtained in nano-powder form. Characterization of nanostructured Zinc oxide powder was carried out using different techniques particularly by SEM, XRD, and UV/ Vis spectroscopy.

4.2.3. Experimental Procedure for the Synthesis of TiO_2/ Nitrogen Doped TiO_2 Nanoparticles by Sonochemical Method

All the analytical grade reagents were used in this experiment including titanium isopropoxide (Daejung), urea (Sigma Aldrich) and 2-propanol (Sigma Aldrich), and no further purification was carried out [29]. Deionized water was used in reaction. Synthesis of Nanocrystalline N-doped anatase TiO_2 was done by sonication of the solution of TPT and urea. In synthesis, mixture of 10.0 ml deionized water and 10.0 ml 2-propanol were used to dislolve 5.0 g urea in a sonication cell. Then 30 ml mixture comprising of 10 ml of TPT and 20 ml isopropyl alcohol was added drop wise into the propanol solution. As reaction is exothermic so apparatus kept in ice bath. The sonication was done under room conditions in the sonication cell. For complete crystallization of TiO_2 reaction was sustained for 150 min. The temperature was limit at 70^0C by circulating water. The centrifugation was carried out to separate the crystal phase then its washing done on filter paper thrice with deionized water and twice by ethanol. The obtained precipitates than placed inside oven overnight for drying. The N-doped TiO_2 synthesized displays pale yellow color after drying.

An undoped TiO_2 was also prepared using same sonochemical method but to avoid N-doping in TiO_2 urea was not dissolved in 2-propanol.

4.3. Characterization of Synthesized Nanoparticles

4.3.1. Characterization of MgO Nanoparticles

Magnesium oxide has been widely studied due to its extraordinary properties, such as high electrical resistivity, chemical inertness, low thermal conductivity and optical transparency [31]. At present, the role of defective sites in MgO is a topic of deep research. MgO Nanoparticles synthesized by sonochemical method were characterized by variety of following characterization techniques:-

4.3.1.1 SEM and EDS of MgO

Particles size, shape and morphology of the synthesized samples of MgO NPs were investigated by using SEM (Scanning electron microscope). The morphology of the synthesized sample was spherical as shown in Figure: 4.4. SEM analysis of MgO was also performed to determine the nanoparticle size and it was revealed that sample particle size ranged from 63.25-98.39 nm. Energy dispersive spectroscopic (EDS) was carried out to investigate the compositions of MgO nanoparticles. Typical EDS spectrum of MgO Nanoparticles is shown in Figure 4.2. Only Mg, and O peaks were detected, which clearly show absence of impurity and any form of transition metal contamination. Table 4.2 shows the consequent atomic % of Mg, and O.

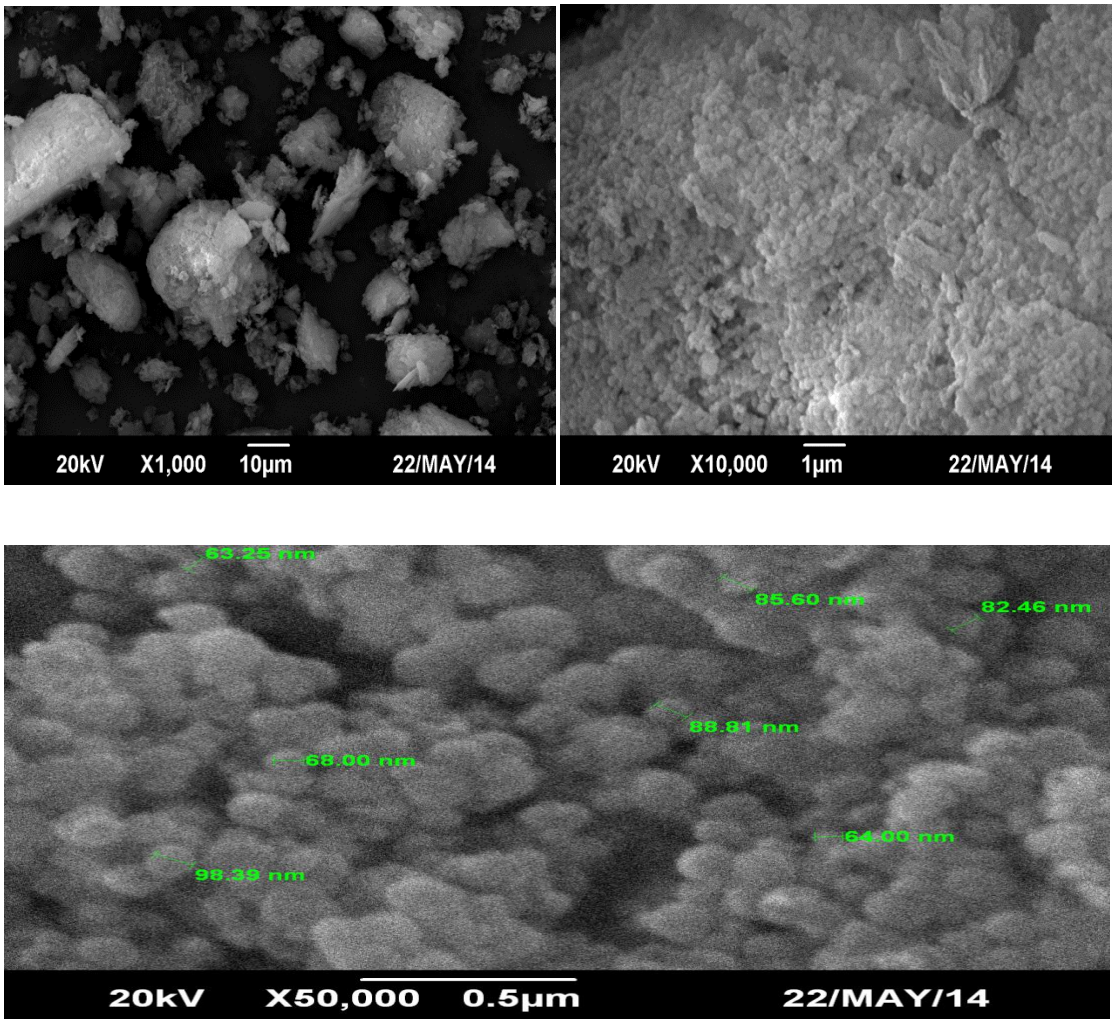

Figure 4.1: SEM Image of MgO Nanoparticles (63.25-98.39 nm)

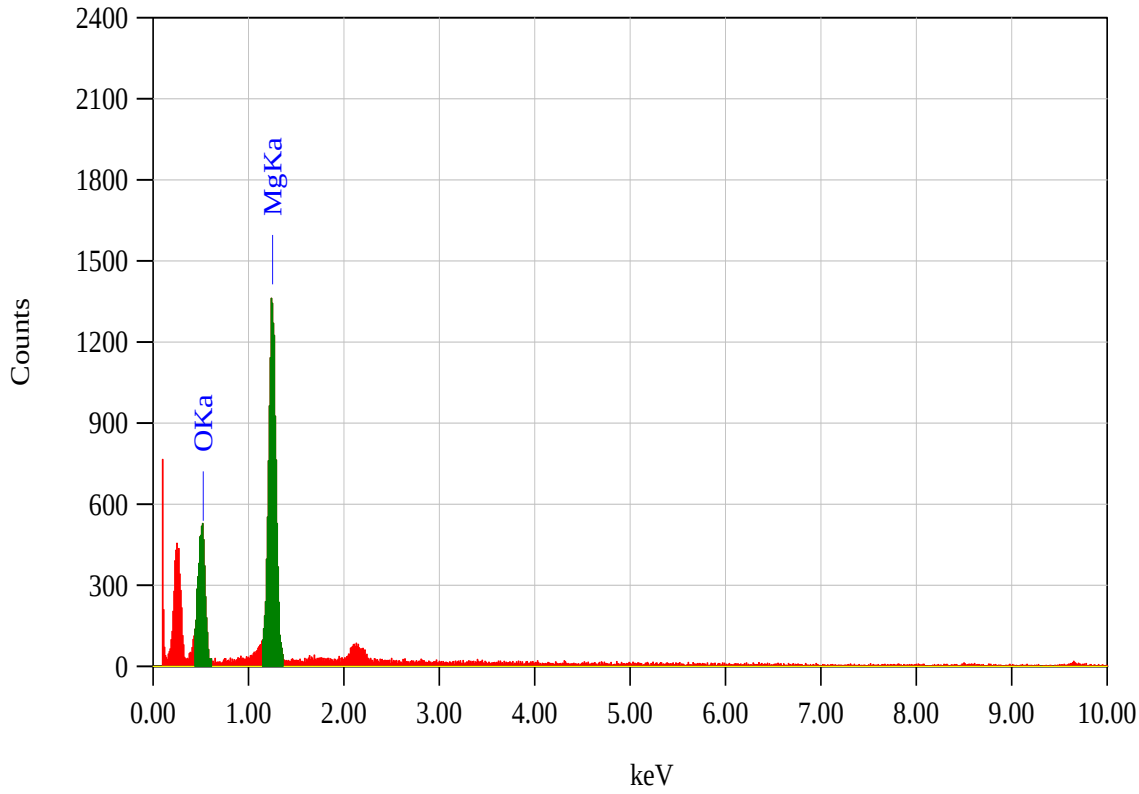

Figure 4.2: EDS Spectrum of MgO NPs

Table 4.2 : EDS Result Of MgO Nanoparticles

Element	Kev	Mass%	Error%	Mol%	Compound	Mass%	K
O K	0.525	39.69		100	MgO	100	100
Mg K	1.253	60.31	1.39				
Total		100.00		100		100	

4.3.1.2 XRD Analysis of MgO Nanoparticles

XRD pattern of MgO Nanoparticles after calcination for 4 hours at a temperature of 400°C is shown in Figure 4.3. It is obvious here that the XRD patterns are fairly the identical and are in complete conformity with the distinctive structure of MgO (Crystal System Cubic, space group Fm-3m, with lattice constants a = 4.2200 Å, Z = 4, Reference Pattern No. 01-075-0447). Good crystallinity of MgO nanoparticles is evident from sharp diffraction peaks as shown in Fig. 4.3. At the same time no characteristic peak linked to any contamination was observed. The broadening of the peaks indicated that the particles were of nanometer scale. Estimated from the sherrer formula, the average size of the particles of sample was 45 nm.

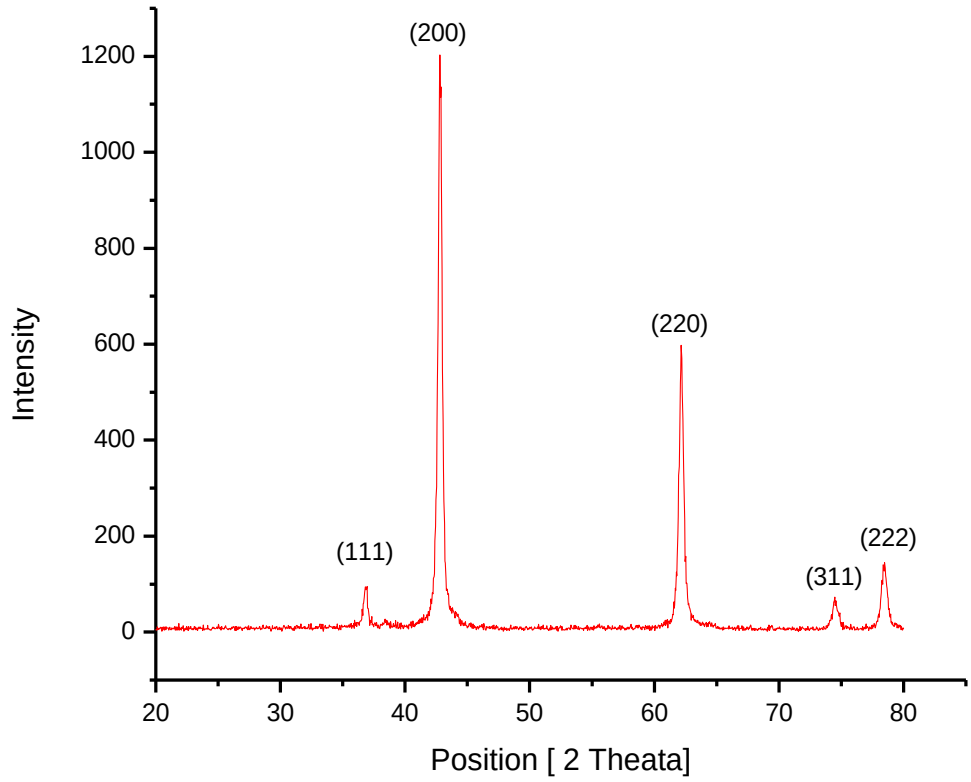

Figure 4.3: XRD Analysis of MgO Showing hkl Values

Visible	Ref. Code	Score	Compound Name	Displacement [°2Th.]	Scale Factor	Chemical Formula
*	01-089-7746	93	Magnesium Oxide	0.000	1.004	Mg O

Fig 4.4: Identified Patterns List

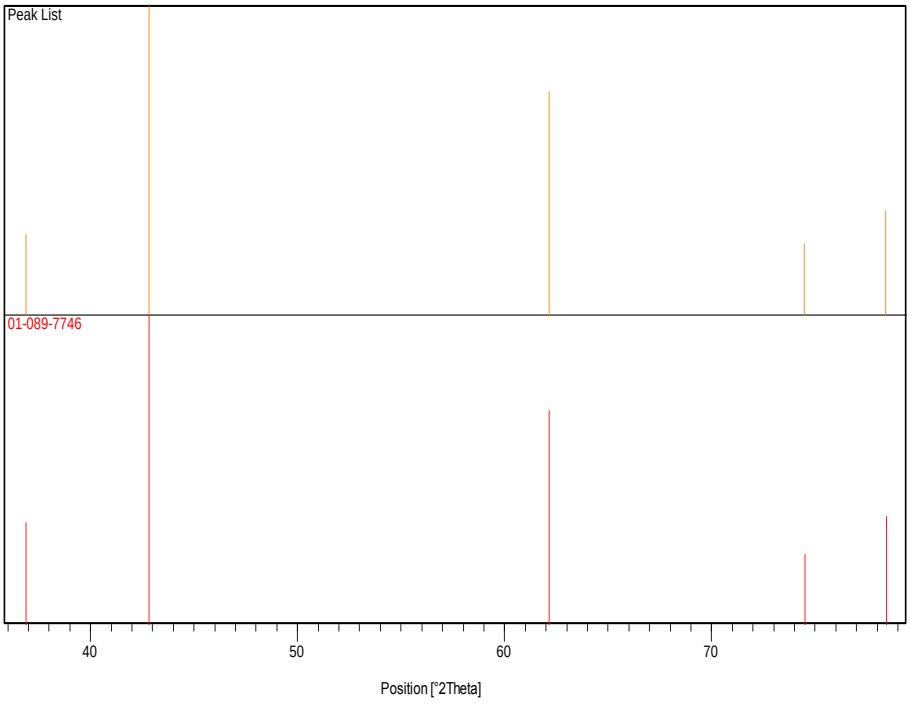

Figure 4.5: Matching Peaks with Stick Pattern

4.3.1.3. PSA of MgO Nanoparticles

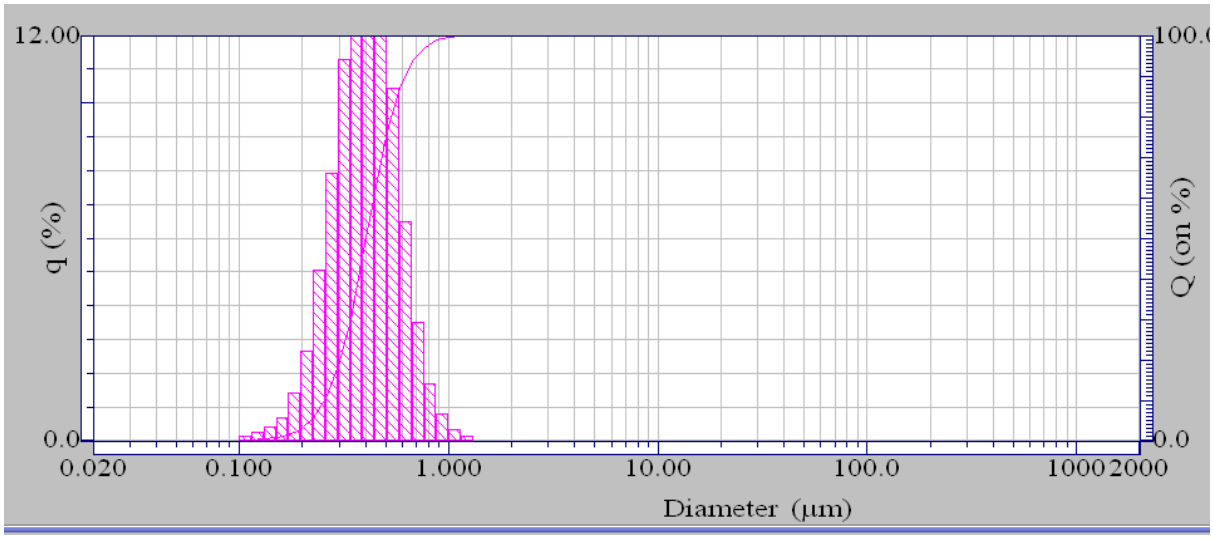

Figure 4.6: PSA of MgO NPs

4.3.2. Characterization of ZnO Nanoparticles

Nanosized ZnO is very attractive II-VI semiconductor material because of its unique properties such as wide band gap (3.37 eV) and large exciton binding energy (60 meV) at room temperature [32]. ZnO nanocrystals have found many applications including solar cells, gas sensors, UV - protection, light emitting diodes etc [33]. ZnO nanoparticles synthesized by sonochemical method were characterized by variety of following characterization techniques:-

4.3.2.1 SEM and EDS of ZnO

Particles size, shape and morphology of the synthesized samples of ZnO NPs were investigated by using SEM (Scanning electron microscope). The morphology of the synthesized sample was cubical as shown in Figure: 4.7. SEM analysis of ZnO was also performed to determine the nanoparticle size and it was revealed that sample particle size ranged from 25-40 nm.

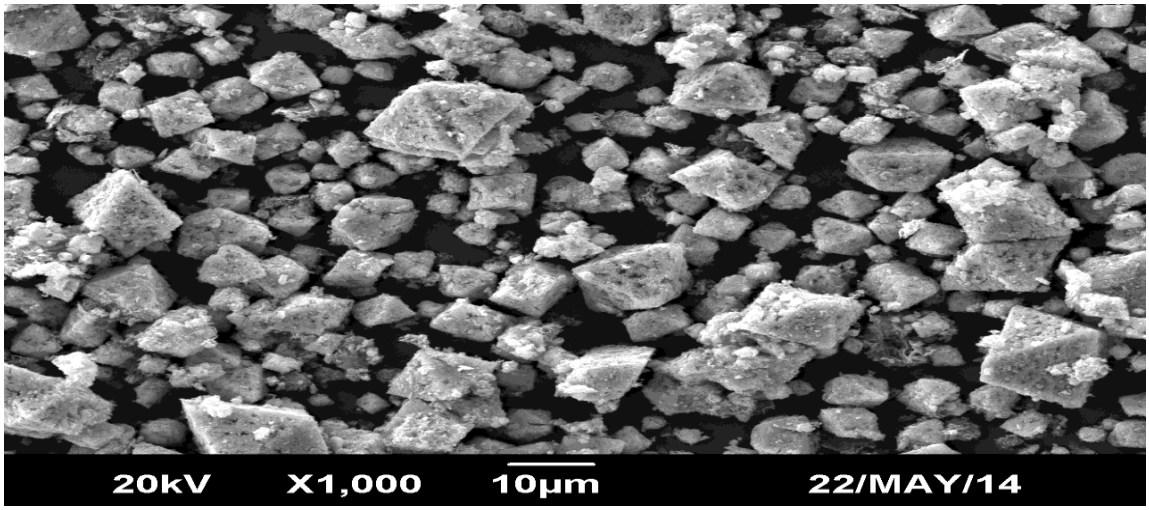

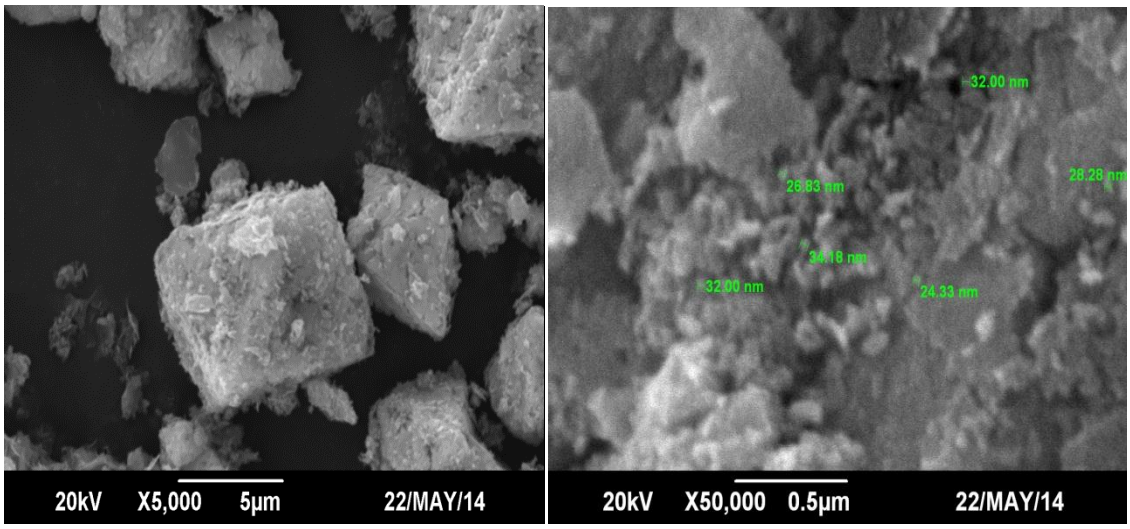

Figure 4.7: SEM Image of ZnO Nanoparticles (25-40 nm)

Figure 4.8. Shows the EDX spectrum of ZnO nanopowders and Table 4.3 shows the ratio of ZnO elemental composition. EDX spectrum shows four peaks which are identified as zinc and oxygen. Hence, it can be seen that pure ZnO nano powders can be prepared using sonochemical method.

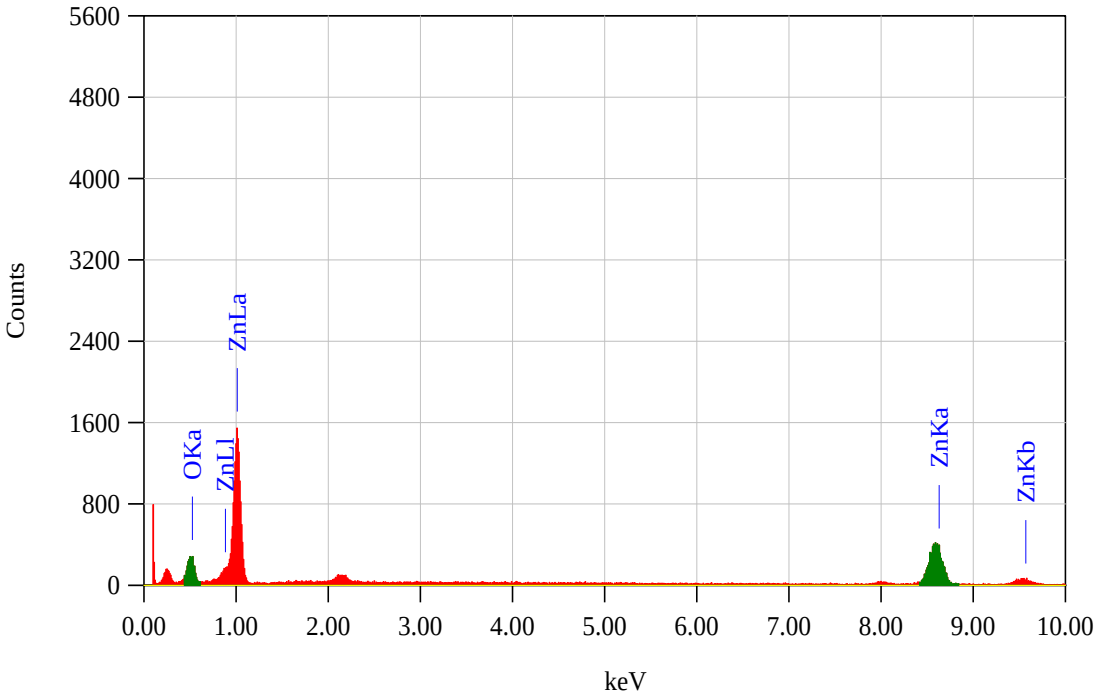

4.8: EDS Spectrum of ZnO NPs

Table 4.3 : EDS Result ZnO Nanoparticles

Element	Kev	Mass%	Error%	Mol%	Compound	Mass%	K
O K	o.525	19.96		100	ZnO	100	100
Zn K	8.630	80.34	3.96				
Total		100.00		100		100	

4.3.2.2. XRD Analysis of Zno NPs

XRD pattern of MgO Nanoparticles after calcinations for 4 hours at a temperature of 400°C is shown in Figure 4.9. It is obvious here that the XRD patterns are fairly identical and are in complete conformity with the wurtzite structure ZnO diffraction (hexagonal phase, space group P63mc, with lattice constants a = 3.2495 Å, c = 1.6021 Å, Z = 2, Reference Pattern No. 01-089-7102). Good crystallinity of ZnO nanoparticles is evident from sharp diffraction peaks as shown in Fig. 4.9. At the same time no characteristic peak linked to any contamination was observed. The broadening of the peaks indicated that the particles were of nanometer scale [34]. Estimated from the sherrer formula, the average size of the particles of sample was 35 nm.

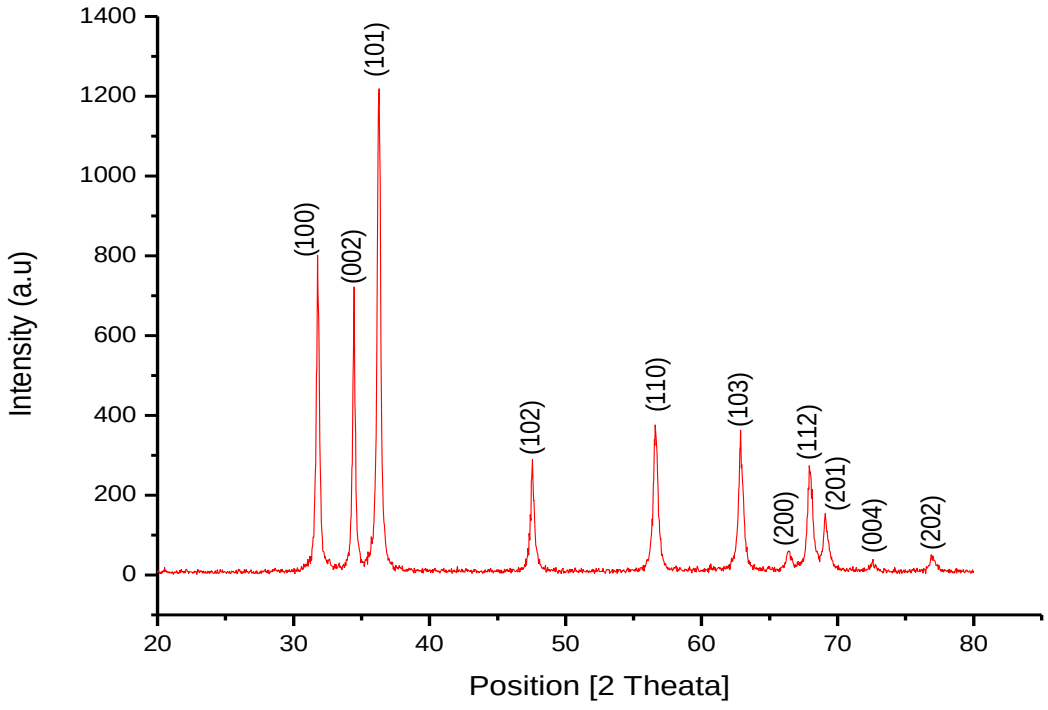

Figure 4.9: XRD Analysis of ZnO Showing hkl Values

Visible	Ref. Code	Score	Compound Name	Displacement [°2Th.]	Scale Factor	Chemical Formula
*	01-089-7102	92	Zincite, syn	0.000	1.082	Zn O

Figure 4.10: Identified Patterns List

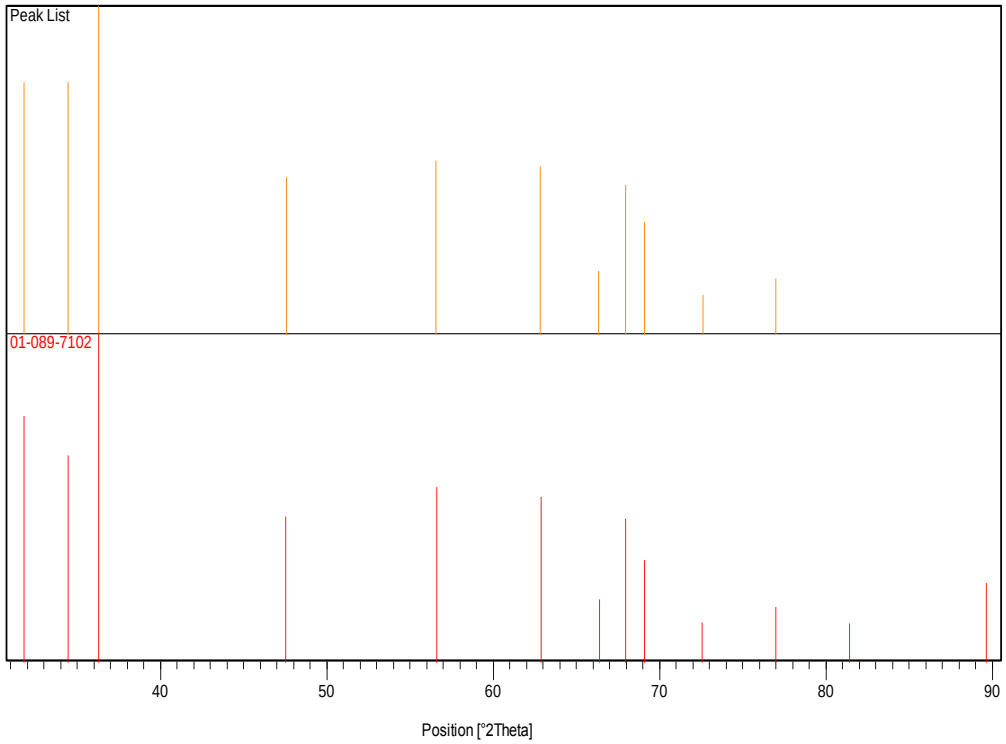

Figure 4.11: Matching Peaks with Stick Pattern

4.3.2.3. PSA of ZnO NPs

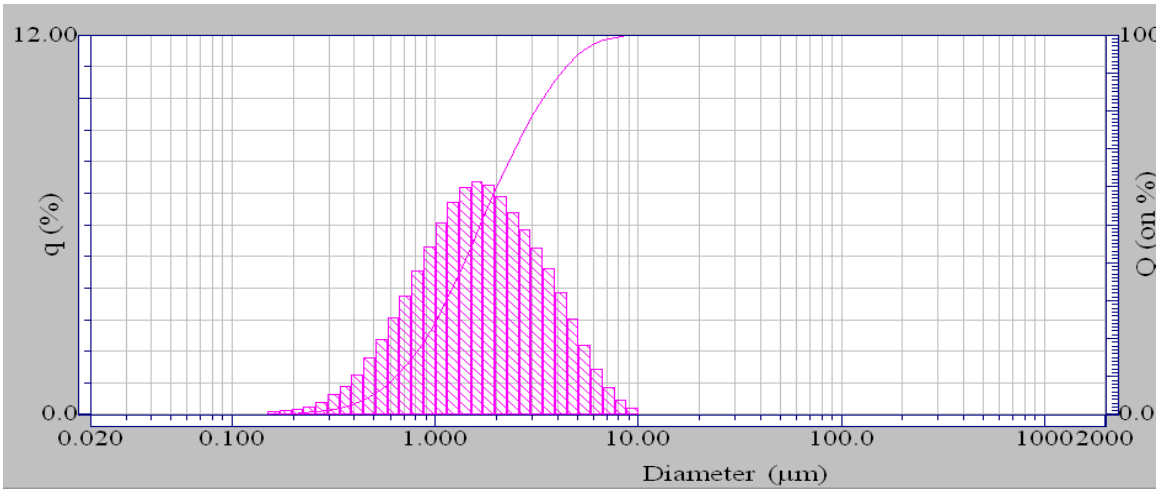

Figure 4.12: PSA of ZnO NPs

4.3.2.4. Reflectance Spectrum of ZnO Bulk and NPs

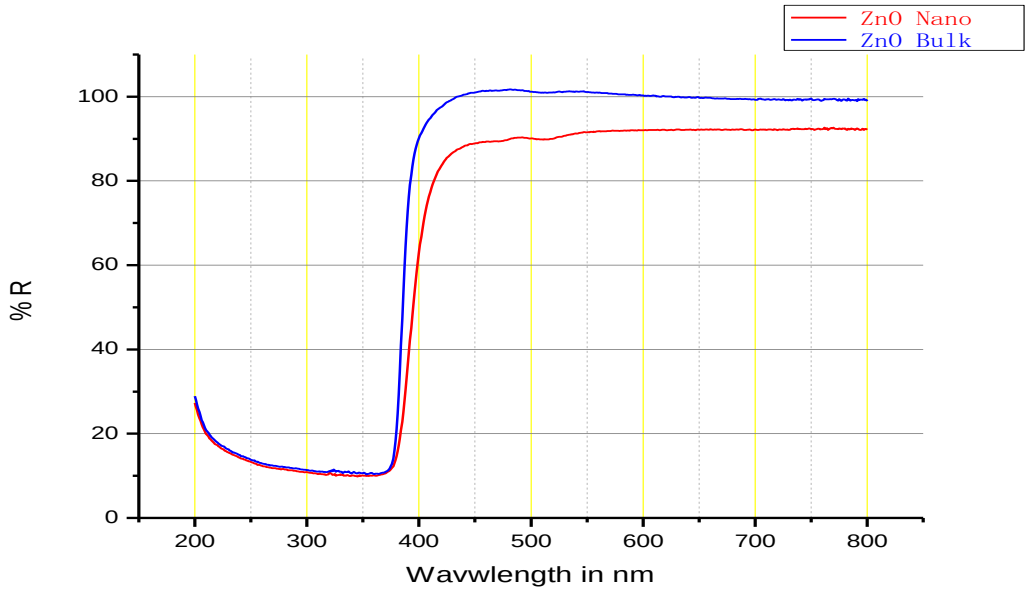

Figure 4.13: Comparative Reflectance Spectrum of ZnO (Bulk & Nano)

4.3.3. Characterization of TiO_2 Nanoparticles

The efficient exploitation of solar energy is one of the foremost goals of contemporary science and engineering as it has a prospect to produce great impact on technological applications [35, 36]. In the list of materials being produced for photocatalytic applications, titanium dioxide (TiO_2) is the most potent candidate because of its almost unmatched efficiency, cheap cost, chemical inertness and photostability.

4.3.3.1. SEM and EDS of TiO_2 NPs

Particles size, shape and morphology of the synthesized samples of TiO_2 NPs were investigated by using SEM (Scanning electron microscope). The morphology of the synthesized sample was spherical as shown in Figure: 4.14. SEM analysis of TiO_2 was also performed to determine the nanoparticle size and it was revealed that sample size ranged from 56-82 nm.

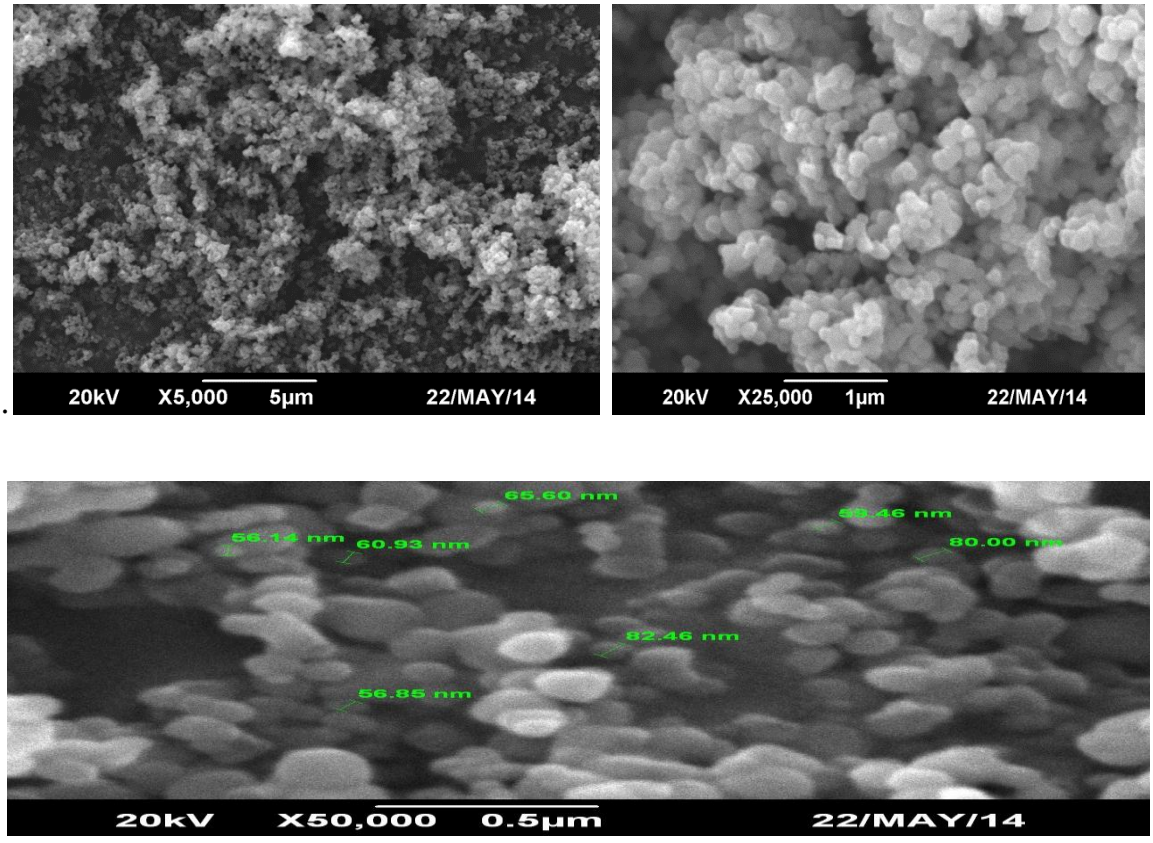

Figure 4.14: SEM Image of TiO_2 Nanoparticles (56-82 nm)

Figure 4.15.shows the EDX spectrum of TiO_2 nanopowders and Table 4.4 shows the ratio of TiO_2 elemental composition. EDX spectrum shows five distinct peaks which are identified as Titanium and oxygen. Hence, it can be seen that pure TiO_2 nano powders can be prepared using sonochemical method for preparation.

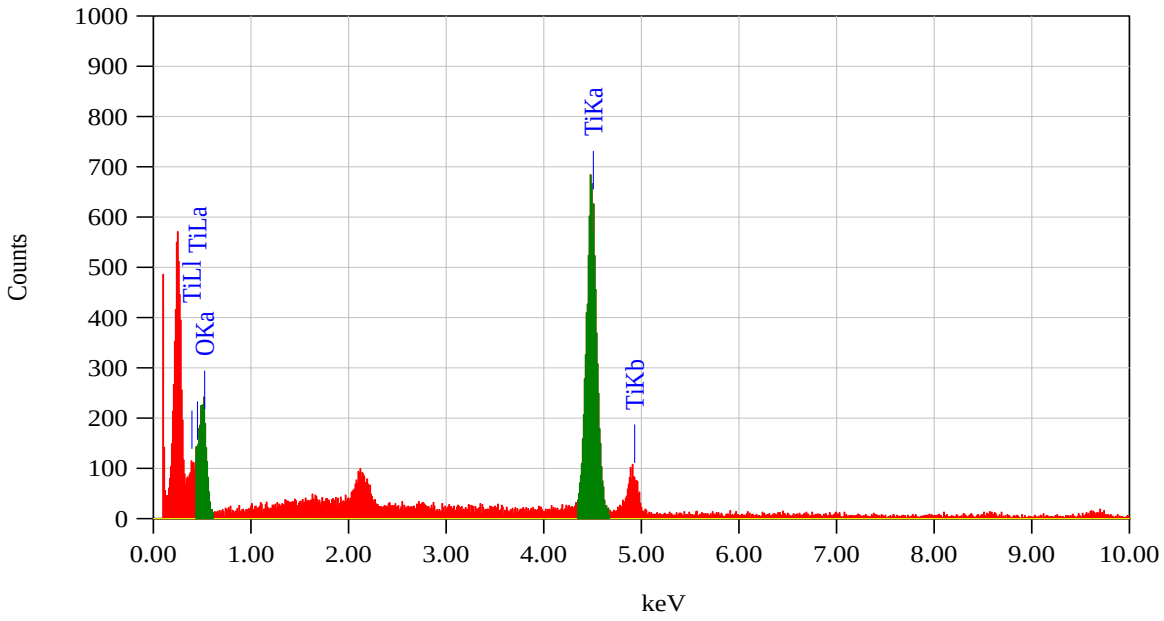

4.15: EDS Spectrum of TiO_2 NPs

Table 4.4 : EDS Result TiO_2 Nanoparticles

Element	**Kev**	**Mass%**	**Error%**	**Mol%**	**Compound**	**Mass%**	**K**
O K	o.525	40.05		100	TiO_2	100	100
Ti K	4.508	59.95	2.66				
Total		100.00		100		100	

4.3.3.2. XRD Analysis of TiO_2 NPs

The formation of titanium dioxide nanoparticles synthesized was supported by X-ray diffraction measurements. Figure 4.16. shows that, XRD analysis showed seven distinct diffraction peaks at 25.3°, 37.8°, 47.9°, 54.5°, 62.8°, 69.5° and 75.1° which indexed the planes 101, 004, 200, 105, 204, 116 and 215 respectively quite the same and are in agreement with the typical structure of TiO_2 (Tetragonal phase, space group l41/amd, with lattice constants a = 3.780 Å, 4 = 2, Reference Pattern No. 01-086-1156). The sharp peaks and absence of unidentified peaks confirmed the crystallinity and higher purity of the prepared nanoparticles.

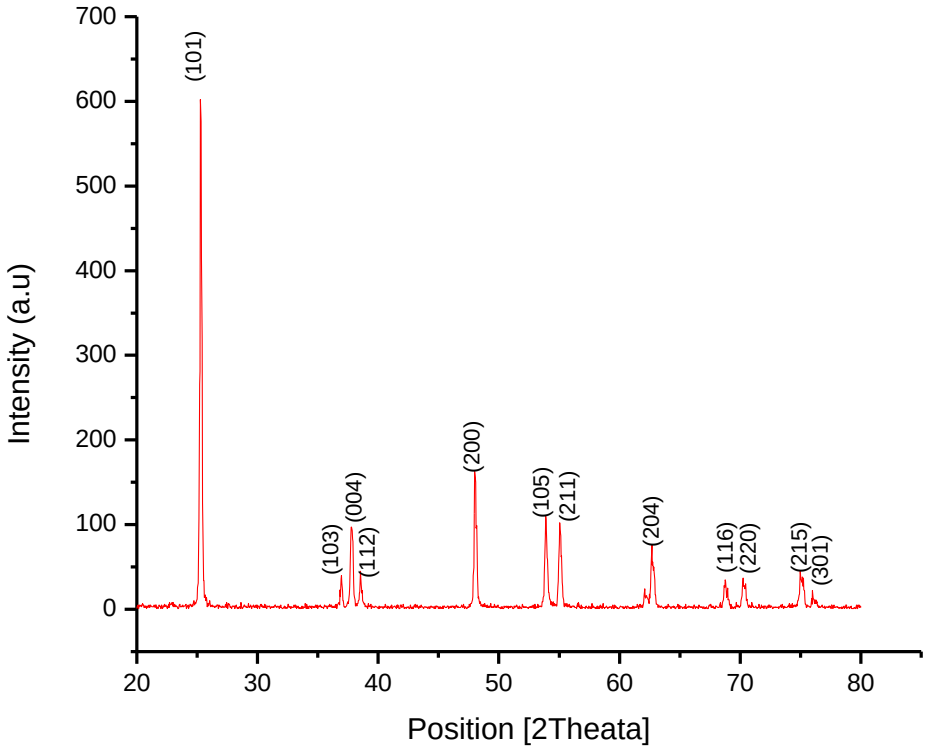

Figure 4.16: XRD Analysis of TiO_2 Showing hkl Values

Visible	Ref. Code	Score	Compound Name	Displacement [°2Th.]	Scale Factor	Chemical Formula
*	03-065-5714	93	Titanium Oxide	0.000	1.008	Ti O2

Figure 4.17: Identified Patterns List

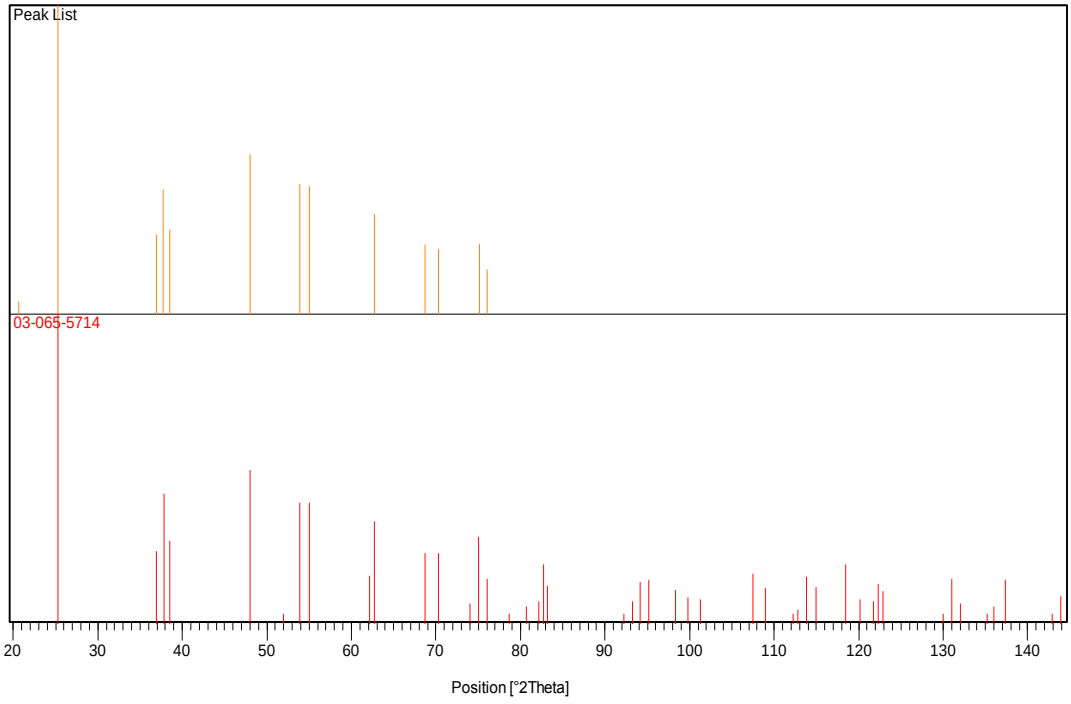

Figure 4.18: Matching Peaks with Stick Pattern

4.3.3.3. PSA of TiO_2 NPs

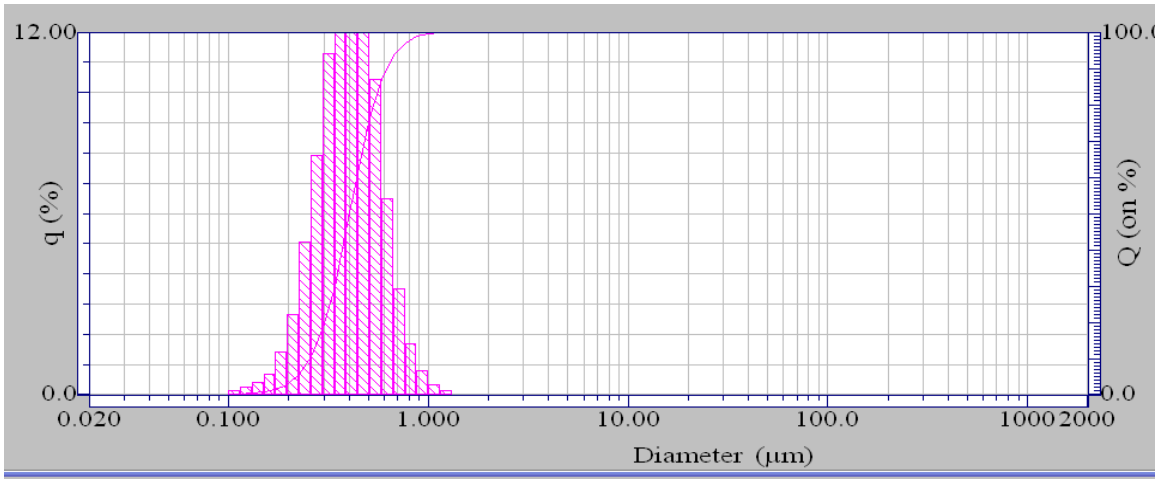

Figure 4.19: PSA of TiO_2 NPs

4.3.4. Characterization of Nitrogen Doped TiO_2 Nanoparticles

TiO_2 is identified as one of the most efficient photocatalysts for the decay of injurious organic pollutants. Though, the band gap of TiO_2 falls in the UV range that means only 4% of sunlight has the sufficient energy to stimulate the catalyst. On the other hand a visible-light stimulated catalyst would be much more effective as it will permit for a much better percentage of sunlight to stimulate the catalyst [37]. Doping TiO_2 with nitrogen has shown a great inclination towards visible-light simualtion because of its comparable atomic size with oxygen, small ionization energy, metastable center formation, and stability.

4.3.4.1. SEM and EDS Analysis of Nitrogen Doped TiO_2

Particles size, shape and morphology of the synthesized samples of N-Doped TiO_2 NPs were investigated by using SEM (Scanning electron microscope). The morphology of the synthesized sample was spherical as shown in Figure: 4.20. SEM analysis of N-Doped TiO_2 was also performed to determine the nano particle size and it was revealed that sample particle size ranged from 63.25-98.39 nm.

Figure 4.21. shows the EDX spectrum of N-Doped TiO_2 nanopowders and Table 4.5 shows the ratio of N-Doped TiO_2 elemental composition. EDX spectrum shows a distinct peak at 0.392 Kev which is identified as Nitrogen. Hence doping of nitrogen in TiO_2 remains successful using sonochemical method for preparation.

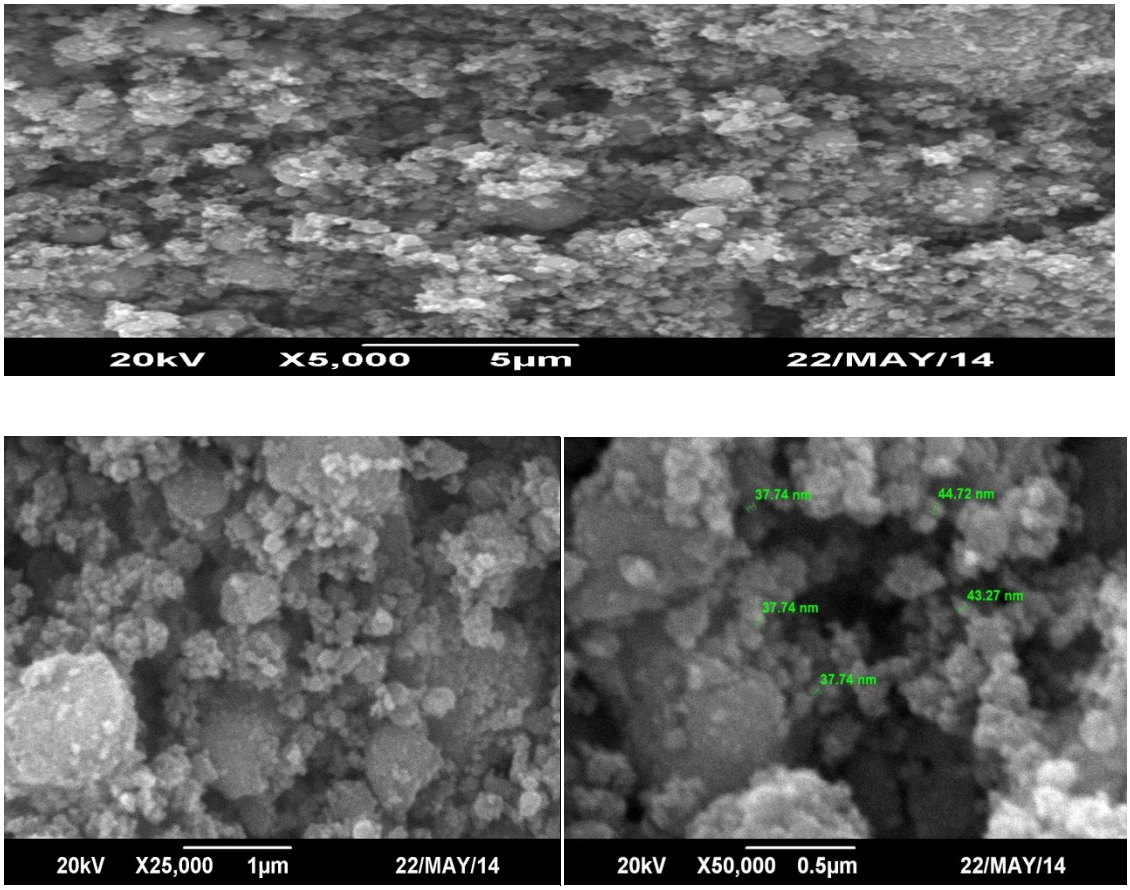

Figure 4.20: SEM Image of Nitrogen Doped TiO_2 Nanoparticles (37-45 nm)

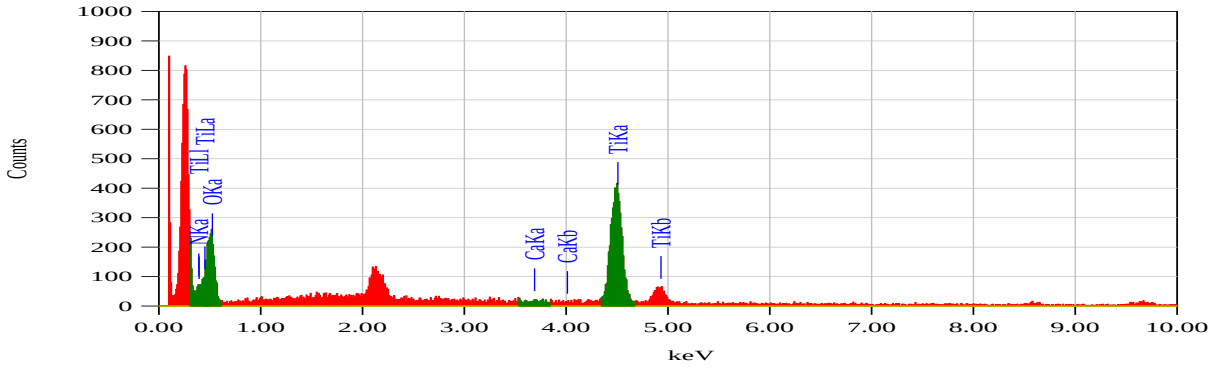

4.21: EDS Spectrum of N-Doped TiO_2 NPs

Table 4.5: EDS Result Nitrogen Doped TiO_2 Nanoparticles							
Element	**Kev**	**Mass%**	**Error%**	**Mol%**	**Compound**	**Mass%**	**K**
N K	0.392	11.42	2.61	42.32	N	11.42	41.2743
O K	0.525	35.42					
Ca K	3.690	0.35	2.81	0.46	CaO	0.49	0.5114
Ti K	4.508	52.81	4.64	57.23	TiO_2	88.09	58.2143
Total		100.00		100		100	

4.3.4.2. XRD Analysis of N-Doped TiO_2 NPs

Figure 4.22 shows the XRD patterns obtained for N-doped TiO_2 nanoparticles synthesized by the sonochemical method. Results showed that the as-prepared particles were comprised of mostly anatase TiO_2 and no separate dopant related phases i.e., TiN, TiON present. In addition, no mixed TiO_2 - TiN phase is indicated by the X-ray diffraction results [38], which signify the nonexistence of an impurity phase. The peaks in the XRD are broad in and this broadness is somehow indication of particles in nanoparticle range [29]. The average crystallite sizes of anatase TiO_2 were calculated from the Debye-Scherrer equation by using the (1 0 1) diffraction peak of TiO_2 anatase, and the average crystalline size of anatase N-TiO_2 was 10.8 nm.

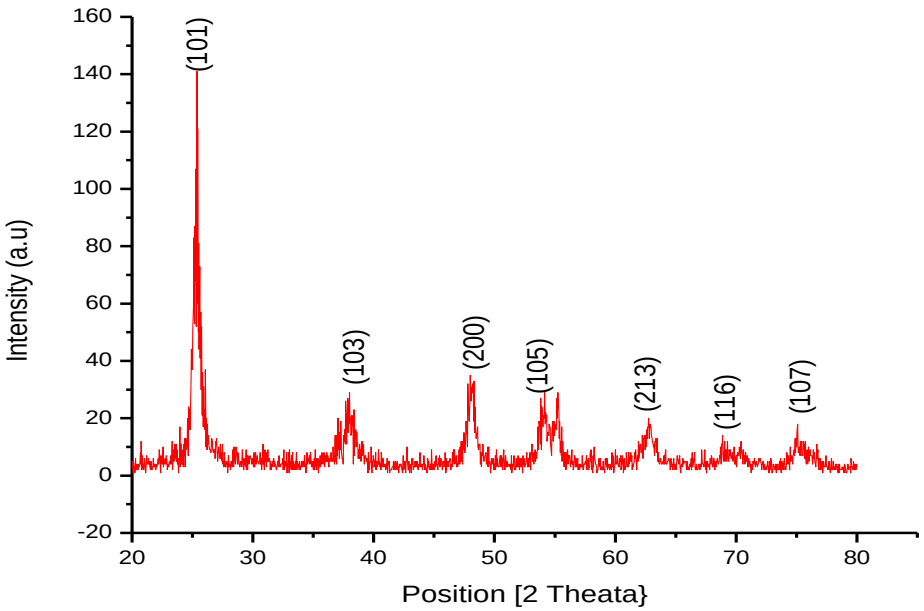

Figure 4.22: XRD Analysis of N-Doped TiO_2 Showing hkl Values

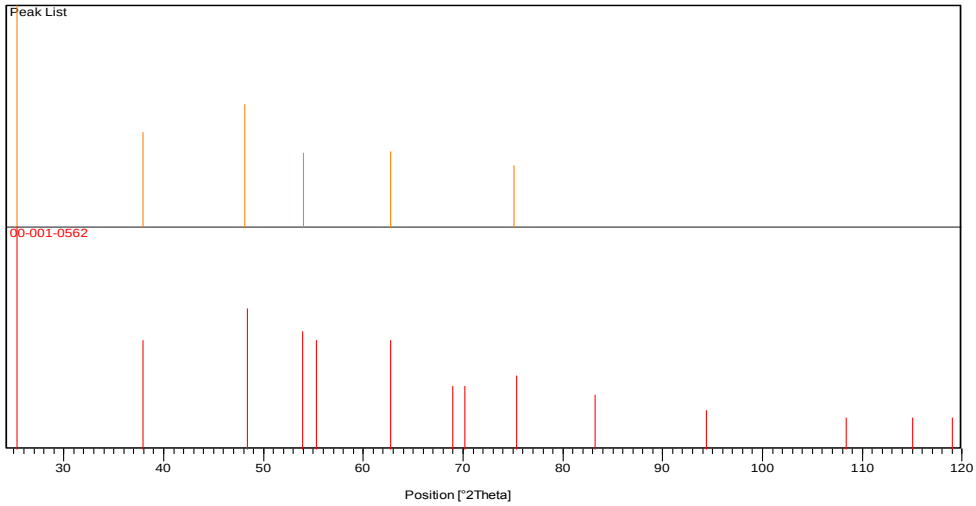

Figure 4.23: Matching Peaks with Stick Pattern

Visible	Ref. Code	Score	Compound Name	Displacement [°2Th.]	Scale Factor	Chemical Formula
*	00-001-0562	52	Anatase	0.000	0.326	Ti O2

Figure 4.24: Identified Patterns List

4.3.4.3. PSA of N-Doped TiO_2 NPs

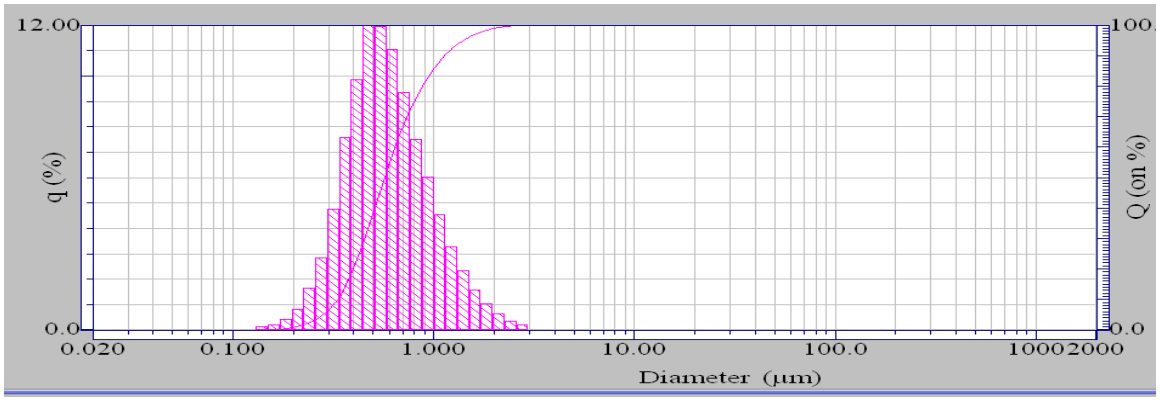

Figure 4.25: PSA of N-Doped TiO_2 NPs

4.3.4.4. Comparative Reflectance Spectrum

Figure. 4.26. shows the UV–vis spectra of the pure Bulk, nano and N-doped TiO_2 nanoparticles. TiO_2 bulk and nano could not absorb visible light, whereas the N-doped TiO_2 showed a distinct absorption in the 400 nm to 700 nm which falls in visible range. This result clearly indicates a decrease in the band gap energy of N–TiO_2. The band gap of the TiO_2 nanocrystallites can be estimated from the intercept of the UV–vis spectra using the following equation [39]:

$$E_g = hc/\lambda \qquad (1)$$

Where E_g is the band gap (eV), h is Planck's constant, c is the light velocity (m/s), and ƛ (nm) is the wavelength of the absorption edge in the spectrum. In the current work, the pure TiO_2 sample exhibited a band energy of 3.21 eV (386 nm), whereas the N-doped TiO_2 samples show a redshift to 2.94 eV (422 nm)[35].

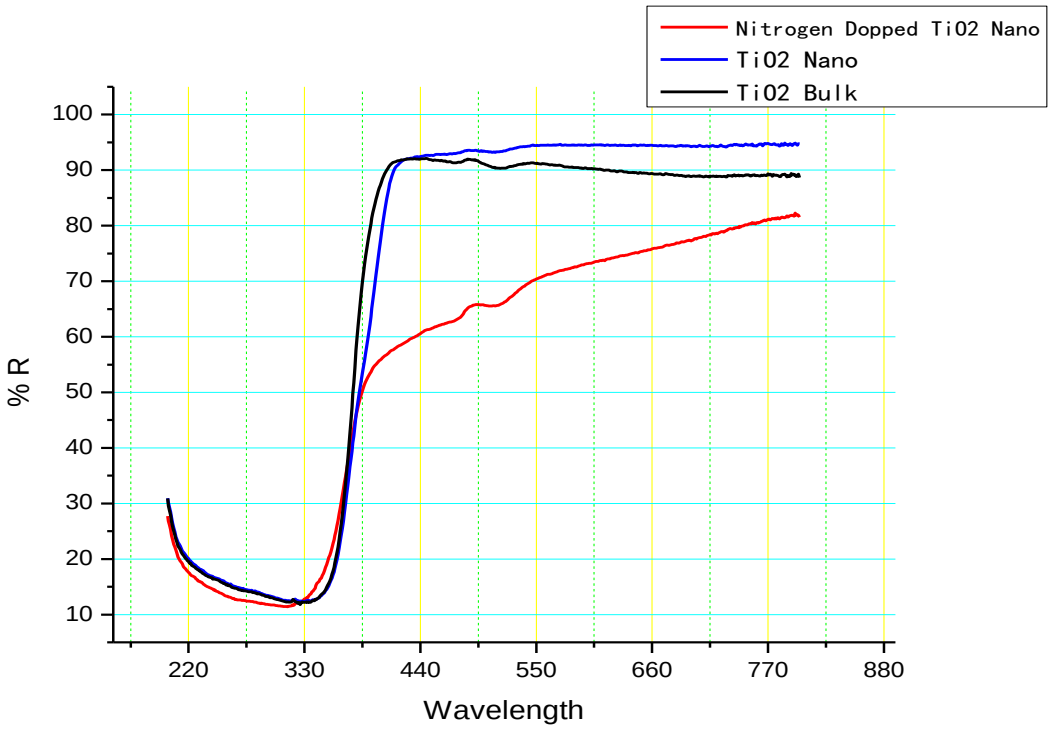

Figure 4.26: Comparative Reflectance Spectrum of TiO_2 (Bulk, Nano & N-Doped)

Chapter 5: Results and Discussion

5. In this part results obtained by the addition of catalyst will be discussed. Comparison of the results will be carried on the basis of their physical condition and their geometry.

5.1. Feed Stock & Catalysts Used

5.1.1. Feed Stock

Following feed stocks were used for analysis under different set of conditions with various catalysts (both Bulk & Nano).

- Pentane
- Hexane
- Heptane
- Naphtha (mixture of Pentane, Hexane & Heptane)

5.1.2. Catalysts Used

Following catalysts were used with feed stock for their cracking under various conditions:-

- Zinc Oxide Bulk
- Titanium Oxide Bulk
- Magnesium Oxide Bulk
- Zinc Oxide NPs
- Titanium Oxide NPs
- Nitrogen Doped Titanium Oxide NPs
- Magnesium Oxide NPs

5.2. Results Obtained with GCMS

Various hydrocarbons with different set of catalysts were placed in Pyrex bottles under different set of conditions and samples were collected using micro syringe characteristically used with GCMS. GCMS used in this research is of SHIMADZU (Japan) GCMS QP 2010 ULTRA. Number of experiments was conducted under various set of conditions however few important results are discussed as under:-

5.2.1. Cracking of Hexane under Sunlight

In this set of experiment hexane was used as feed stock and kept under sunlight for different duration of time i.e 4, 8 and 12 hours. Both bulk and nano catalysts were used to ascertain the decomposition products using GCMS. Few of the observations made during experiment are as under:-

1. **Reference ser 1 table 5.1.** Pure hexane sample used as standard does not decompose even after its exposure to sunlight for 12 hrs
2. **Reference ser 2 table 5.1.** 50 mg TiO_2 bulk was poured into 30 ml feedstock. After 4 hrs sample was collected and made to undergo GCMS but there were no decomposition products detected. However after 8 hrs 3-methyl Pentane detected along with base peek of hexane.
3. **Reference ser 3 table 5.1** 50 mg TiO_2 nanoparticles were poured into 30 ml feedstock. After 4 hrs sample was collected and made to undergo GCMS but there were no decomposition products detected. However after 8 hrs 3-methyl Pentane and cyclopentane methyle were detected along with base peek of hexane.
4. **Reference ser 4 table 5.1** 50 mg Nitrogen doped TiO_2 nanoparticles were poured into 30 ml feedstock. After 4 hrs sample was collected and made to undergo GCMS traces of butane, 2 methyl were detected along hexane. After 12 hrs in addition traces of Butane,2,2,3-trimethyl were also detected along with base peek of hexane.
5. **Reference ser 5 table 5.1** 50 mg ZnO bulk was poured into 30 ml feedstock. After 4 hrs sample was collected and made to undergo GCMS only hexane

detected. However after 12 hrs in addition traces of 3-methyl Pentane and cyclopentane methyl were also detected along with base peek of hexane.

6. **Reference ser 6 table 5.1** 50 mg ZnO nanoparticles were poured into 30 ml feedstock. After 4 hrs sample was collected and made to undergo GCMS, 3-methyl Pentane in addition to hexane detected. However after 12 hrs traces of 3-methyl Pentane and cyclopentane methyl were also detected along with base peek of hexane.
7. **Reference ser 7 table 5.1** 50 mg MgO bulk was poured into 30 ml feedstock. After 4 hrs sample was collected and made to undergo GCMS but there were no decomposition products detected. Even after 8 hrs no decomposition observed.
8. **Reference ser 8 table 5.1** 50 mg MgO nanoparticles were poured into 30 ml feedstock. After 4 hrs sample was collected and made to undergo GCMS but there were no decomposition products detected. However after 8 hrs traces of 3-methyl Pentane were also observed along with hexane.

Table 5.1 : Hexane under Sunlight

Ser	**Feed stock (30 ml)**	**Catalyst (50 mg)**	**Time Hrs**	**GCMS Peaks**
1	**Hexane**	**Nil (Standard)**	12	n-Hexane
2	"	TiO_2 Bulk	4	n-Hexane
			8	n-Hexane, 3-methyl Pentane(3MP)
3	"	TiO_2 Nano	4	n-Hexane
			8	n-Hexane

				3-methyl Pentane Cyclopentane methyl
4	“	N-Doped TiO_2 Nano	4	n-Hexane Butane,2 methyl / isopentane,
			8	n-Hexane , 3-methyl Pentane
			12	n-Hexane, 3-methyl Pentane, Butane,2,2,3-trimethyl
5	“	ZnO Bulk	4	n-Hexane
			8	n-Hexane , 3-methyl Pentane, Cyclopentane methyl,
6	“	ZnO Nano	4	n-Hexane , 3-methyl Pentane
			8	n-Hexane, 3-methyl Pentane, Cyclopentane methyl
			12	n-Hexane , 3-methyl Pentane, Cyclopentane methyl
7	“	MgO Bulk	4	n-hexane
			8	n-hexane
8	“	MgO Nano	4	n-hexane
			8	n-hexane 3-methyl Pentane

5.2.2. Cracking of Heptane under Sunlight

In this set of experiment heptane was used as feed stock and kept under sunlight for different duration of time i.e 4, 8 and 12 hours. Both bulk and nano catalysts were used to ascertain the decomposition products using GCMS. Few of the observations made during experiment are as under:-

1. **Reference ser 1 table 5.2.** Pure heptane sample used as standard it does not decompose even after its exposure to sunlight for 8 hrs.
2. **Reference ser 2 table 5.2.** 50 mg TiO_2 bulk was poured into 30 ml feedstock. After 8 hrs sample was collected and made to undergo GCMS but there were no decomposition products detected.
3. **Reference ser 3 table 5.2.** 50 mg TiO_2 nanoparticles were poured into 30 ml feedstock. After 8 hrs traces of 2-ethylpentane were detected along with base peek of heptane.
4. **Reference ser 4 table 5.2.** 50 mg Nitrogen doped TiO_2 nanoparticles were poured into 30 ml feedstock. After 8 hrs traces of cyclohexanemethane and 2-ethylpentane were also detected along with base peek of heptane.
5. **Reference ser 5 table 5.2.** 50 mg ZnO bulk was poured into 30 ml feedstock. After 8 hrs sample was collected and made to undergo GCMS but there were no decomposition products detected.
6. **Reference ser 6 table 5.2.** 50 mg ZnO nanoparticles were poured into 30 ml feedstock. After 8 hrs sample taken was tested using GCMS and traces of 2ethylpentane were detected along with heptanes itself.
7. **Reference ser 7 table 5.2.** 50 mg MgO bulk was poured into 30 ml feedstock. After 8 hrs sample was collected and made to undergo GCMS but there were no decomposition products detected.
8. **Reference ser 8 table 5.2.** 50 mg MgO nanoparticles were poured into 30 ml feedstock. After 8 hrs sample taken was tested using GCMS and traces of 2ethylpentane were detected along with heptanes itself.

Table 5.2 : Heptane under Sunlight				
Ser	**Feed stock (30 ml)**	**catalyst (50 mg)**	**Time Hrs**	**GCMS Peaks**
1	**Heptane**	**Nil (Standard)**	8	n-heptane
2	“	TiO_2 Bulk	8	n-heptane
3	“	TiO_2 Nano	8	n-heptane Hexane, 3 methyl/ 2ethylpentane
4	“	TiO_2 Nitrogen Doped Nano	8	n-heptane cyclohexanemethane Hexane, 3 methyl/ 2ethylpentane
5	“	ZnO Bulk	8	n-heptane
6	“	ZnO Nano	8	n-heptane hexane,3 methyl/ 2ethylpentane
7	“	MgO Bulk	8	n-heptane
8	“	MgO Nano	8	n-heptane hexane, 3 methyl/ 2ethylpentane

5.2.3. Cracking of Naphtha under Sunlight

In this set of experiment Naphtha (pentane, hexane and heptanes) was used as feed stock and kept under sunlight for different duration of time i.e 4, 8 and 12 hours. Both bulk and nano catalysts were used to ascertain the decomposition products using GCMS. Few of the observations made during experiment are as under:-

1. **Reference ser 1 table 5.3.** Naphtha sample used as standard without any catalyst. On GCMS signals detected were of its constituents only.
2. **Reference ser 2 table 5.3.** 50 mg TiO_2 bulk was poured into 30 ml feedstock. After 8 hrs sample was collected and made to undergo GCMS but there were no decomposition products detected.
3. **Reference ser 3 table 5.3.** 50 mg TiO_2 nanoparticles were poured into 30 ml feedstock. After 8 hrs traces of 3-methylpentane were detected along with peeks of naphtha constituents.
4. **Reference ser 4 table 5.3.** 50 mg Nitrogen doped TiO_2 nanoparticles were poured into 30 ml feedstock. After 8 hrs traces of Butane,2,3-dimethyl and Butane,2,2,3-trimethyl were also detected.
5. **Reference ser 5 table 5.3.** 50 mg ZnO bulk was poured into 30 ml feedstock. After 8 hrs sample was collected and made to undergo GCMS but there were no decomposition products detected. On GCMS signals detected were of naphtha constituents only
6. **Reference ser 6 table 5.3.** 50 mg ZnO nanoparticles were poured into 30 ml feedstock. After 8 hrs traces of Butane,2,2,3-trimethyl were detected.
7. **Reference ser 7 table 5.3.** 50 mg MgO bulk was poured into 30 ml feedstock. After 8 hrs sample was collected and made to undergo GCMS but there were no decomposition products detected.
8. **Reference ser 8 table 5.3.** 50 mg MgO nanoparticles were poured into 30 ml feedstock. After 8 hrs sample was collected and made to undergo GCMS but there were no decomposition products detected.

Table 5.3 : Naphtha under Sunlight				
Ser	**Feed stock (30 ml)**	**Catalyst (50 mg)**	**Time Hrs**	**GCMS Peaks**
1	**Naphtha**	**Nil (Standard)**	8	n-Pentane, n-Hexane, n-Heptane
2	“	TiO_2 Bulk	8	n-Pentane, n-Hexane, n-Heptane
3	“	TiO_2 Nano	8	n-Pentane, n-Hexane, n-Heptane Pentane, 3 Methyl/ 3-methylpentane
4	“	TiO_2 Nitrogen Doped Nano	8	n-Pentane, n-Hexane, n-Heptane Butane,2,3-dimethyl Butane,2,2,3-trimethyl
5	“	ZnO Bulk	8	n-Pentane, n-Hexane n-Heptane
6	“	ZnO Nano	8	n-Pentane, n-Hexane, n-Heptane Butane,2,2,3-trimethyl
7	“	MgO Bulk	8	n-Pentane, n-Hexane, n-Heptane
8	“	MgO Nano	8	n-Pentane, n-Hexane, n-Heptane

5.2.4. Cracking of Hexane under UV Light

In this set of experiment hexane was used as feed stock and kept under UV 366 nm for 2 hrs. Both bulk and nano catalysts were used to ascertain the decomposition products using GCMS. Few of the observations made during experiment are as under:-

1. **Reference ser 1 table 5.4.** Hexane sample used as standard without any catalyst. No peak detected other than hexane itself.
2. **Reference ser 2 table 5.4.** 50 mg TiO_2 bulk was poured into 30 ml feedstock. After 2 hrs sample was collected and made to undergo GCMS but there were no decomposition products detected.
3. **Reference ser 3 table 5.4.** 50 mg TiO_2 nanoparticles were poured into 30 ml feedstock. After 2 hrs traces of 3-methylpentane were detected along with base peek of hexane.
4. **Reference ser 4 table 5.4.** 50 mg Nitrogen doped TiO_2 nanoparticles were poured into 30 ml feedstock. After 2 hrs traces of cyclobutane, Ethyl and 3-methylpentane were detected.
5. **Reference ser 5 table 5.4.** 50 mg ZnO bulk was poured into 30 ml feedstock. After 2 hrs sample was collected and made to undergo GCMS. Traces of 3-methylpentane in addition to n-hexane were observed.
6. **Reference ser 6 table 5.4.** 50 mg ZnO nanoparticles were poured into 30 ml feedstock. After 2 hrs traces of butane,2,2,3-trimethyl and cyclohexane were detected on GCMS.
7. **Reference ser 7 table 5.4.** 50 mg MgO bulk was poured into 30 ml feedstock. After 2 hrs sample was collected and made to undergo GCMS but there were no decomposition products detected.
8. **Reference ser 8 table 5.4.** 50 mg MgO nanoparticles were poured into 30 ml feedstock. After 2 hrs sample was collected and made to undergo GCMS. Traces of methylcyclopentane in addition to n-hexane were observed.

Table 5.4 : Hexane under UV 366 nm				
Ser	**Feed stock (30 ml)**	**Catalyst (50 mg)**	**Time Hrs**	**GCMS Peaks**
1	**Hexane**	**Nil (Standard)**	2	**n-hexane**
2	“	TiO_2 Bulk	2	n-hexane
3	“	TiO_2 Nano	2	n-hexane, 3-Methylpentane
4	“	TiO_2 Nitrogen Doped Nano	2	n-hexane, 3-Methylpentane Cyclobutane, Ethyl
5	“	ZnO Bulk	2	n-hexane, 3-Methylpentane
6	“	ZnO Nano	2	n-hexane, cyclohexane butane,2,2,3-trimethyl
7	“	MgO Bulk	2	n-hexane
8	“	MgO Nano	2	n-hexane methylcyclopentane

5.2.5. Cracking of Heptane under UV Light

In this set of experiment hexane was used as feed stock and kept under UV 366 nm for 2 hrs. Both bulk and nano catalysts were used to ascertain the decomposition products using GCMS. Few of the observations made during experiment are as under:-

1. **Reference ser 1 table 5.5.** Heptane sample used as standard without any catalyst. No peak detected other than heptane itself.
2. **Reference ser 2 table 5.5.** 50 mg TiO_2 bulk was poured into 30 ml feedstock. After 2 hrs sample was collected and made to undergo GCMS but there were no decomposition products detected.
3. **Reference ser 3 table 5.5.** 50 mg TiO_2 nanoparticles were poured into 30 ml feedstock. After 2 hrs traces of 2-ethylpentane were detected along with base peek of heptane.
4. **Reference ser 4 table 5.5.** 50 mg Nitrogen doped TiO_2 nanoparticles were poured into 30 ml feedstock. After 2 hrs traces of Cyclohexane, methyl and 2-ethylpentane were detected.
5. **Reference ser 5 table 5.5.** 50 mg ZnO bulk was poured into 30 ml feedstock. After 2 hrs sample was collected and made to undergo GCMS but there were no decomposition products detected
6. **Reference ser 6 table 5.5.** 50 mg ZnO nanoparticles were poured into 30 ml feedstock. After 2 hrs traces of Cyclohexane, methyl and 2-ethylpentane were detected on GCMS.
7. **Reference ser 7 table 5.5.** 50 mg MgO bulk was poured into 30 ml feedstock. After 2 hrs sample was collected and made to undergo GCMS but there were no decomposition products detected.
8. **Reference ser 8 table 5.5.** 50 mg MgO nanoparticles were poured into 30 ml feedstock. After 2 hrs sample was collected and made to undergo GCMS. Traces of 2-ethylpentane in addition to n-hexane were observed on GCMS.

Table 5.5 : Heptane under UV 366 nm				
Ser	**Feed stock (30 ml)**	**Catalyst (50 mg)**	**Time Hrs**	**GCMS Peaks**
1	**Heptane**	**Nil (Standard)**	2	n-heptane
2	“	TiO_2 Bulk	2	n-heptane
3	“	TiO_2 Nano	2	n-heptane Hexane, 3 methyl/ 2ethylpentane
4	“	TiO_2 Nitrogen Doped Nano	2	n-heptane Hexane, 3 methyl/ 2ethylpentane Cyclohexane , methyl
5	“	ZnO Bulk	2	n-heptane
6	“	ZnO Nano	2	n-heptane Hexane, 3 methyl/2 ethylpentane Cyclohexane , methyl
7	“	MgO Bulk	2	n-heptane
8	“	MgO Nano	2	n-heptane Hexane, 3 methyl/ 2ethylpentane

5.2.6. Cracking of Naphtha under UV Light

In this set of experiment Naphtha (pentane, hexane and heptanes) was used as feed stock and kept under UV 366 nm for 2 hrs. Both bulk and nano catalysts were used to ascertain the decomposition products using GCMS. Few of the observations made during experiment are as under:-

1. **Reference ser 1 table 5.6.** Naphtha sample used as standard without any catalyst. On GCMS signals detected were of its constituents only.
2. **Reference ser 2 table 5.6.** 50 mg TiO_2 bulk was poured into 30 ml feedstock. After 2 hrs sample was collected and made to undergo GCMS but there were no decomposition products detected.
3. **Reference ser 3 table 5.6.** 50 mg TiO_2 nanoparticles were poured into 30 ml feedstock. After 2 hrs traces of Butane,2,2,3-trimethyl were detected along with peeks of naphtha constituents.
4. **Reference ser 4 table 5.6.** 50 mg Nitrogen doped TiO_2 nanoparticles were poured into 30 ml feedstock. After 2 hrs traces of 3,4-dimethylheptane in addition to peeks of naphtha constituents was also detected.
5. **Reference ser 5 table 5.6.** 50 mg ZnO bulk was poured into 30 ml feedstock. After 2 hrs sample was collected and made to undergo GCMS but there were no decomposition products detected. On GCMS signals detected were of naphtha constituents only
6. **Reference ser 6 table 5.6.** 50 mg ZnO nanoparticles were poured into 30 ml feedstock. After 2 hrs traces of Butane,2,3-dimethyl were detected.
7. **Reference ser 7 table 5.6.** 50 mg MgO bulk was poured into 30 ml feedstock. After 2 hrs sample was collected and made to undergo GCMS but there were no decomposition products detected.
8. **Reference ser 8 table 5.6.** 50 mg MgO nanoparticles were poured into 30 ml feedstock. After 8 hrs sample was collected and made to undergo GCMS but there were no decomposition products detected.

Table 5.6 : Naphtha under UV 366 nm				
Ser	**Feed stock (30 ml)**	**catalyst (50 mg)**	**Time Hrs**	**GCMS Peaks**
1	**Naphtha**	**Nil (Standard)**	2	n-pentane n-hexane, .n-heptane
2	“	TiO_2 Bulk	2	n-pentane, .n-hexane, .n-heptane
3	“	TiO_2 Nano	2	n-pentane, .n-hexane, .n-heptane Butane,2,2,3-trimethyl
4	“	TiO_2 Nitrogen Doped Nano	2	n-pentane, n-hexane, n-heptane 3,4-dimethylheptane
5	“	ZnO Bulk	2	n-pentane, n-hexane, n-heptane
6	“	ZnO Nano	2	n-pentane, n-hexane, n-heptane, Butane,2,3-dimethyl
7	“	MgO Bulk	2	n-pentane, n-hexane, n-heptane
8	“	MgO Nano	2	.n-pentane, .n-hexane, .n-heptane

5.3. Discussion on Results

After going through all the results few deductions can be made for understanding the wide variety of results obtained while using different conditions and different set of catalysts.

5.3.1. Results Obtained under Sunlight

It can be easily made out after going through the results that most of time while using bulk catalysts decomposition products were either not produced or minimum. However when nanocatalysts were used these produce a wide range of results but at least these were better as compared to bulk catalysts. Here we can conclude some important results as under:-

1. Better results displayed by nanocatalysts as compared to bulk catalysts because of low volume to surface ratio of its particles or in other words due to their exceptionally minute size (typically 10–80 nm) that produces a great surface area-to-volume ratio.
2. TiO_2 have band gap energy equal to 3.21 eV which warrants the photon from uv spectrum range to cause excitation between conduction and valance band. But when it was doped with N samples show a redshift to 2.94 eV (422 nm). Hence can produce activity under spectrum of visible light and the same we have observed in our experiments under sunlight as we have gained the best results while using N-doped TiO_2.
3. ZnO almost have band gap energy equals to 3.37 eV (367 nm) and also falls in the uv sensitive region. It is quite obvious from results as well that limited activity is being displayed by ZnO nanoparticles.
4. MgO have larger band gap energy and does not fall in the category of photo catalysts but intently used in these experiments to give a comparison between catalysts of photosensitive and non photosensitive nature. Here we can see results displayed by this catalyst are very low.

5.3.2. Results Obtained under UV Spectrum 366 nm

Extensive tests were undertaken using UV lamp 366 nm. In this set of experiments few additional observations are made as under:-

1. Wavelength of uv light produced by this lamp is almost equal to that of ZnO. Hence energy carried by these photons (3.39 eV) is slightly greater than the energy required to cause excitation in this photocatalyst. Careful study of experimental results further augment this idea as the best results were achieved while using ZnO nanoparticles.
2. Catalysts in bulk form were not as efficient as nanocatalysts for the same reason as mentioned earlier.
3. TiO_2 and N-doped TiO_2 which require 3.21 eV and 2.94 eV[35] energy respectively for excitation across the bands also produced satisfactory results.

Chapter 6: Conclusions with Future Prospects

6. This chapter explains the final outcome of the study and the further work which may be carried in future.

6.1. **Conclusions**

- MgO, ZnO and TiO_2 nano catalysts were synthesized and categorized using various characterization techniques (SEM, XRD and PSA).

- Catalysts were used in bulk and in nano form for comparative study.

- More quality and quantity of cracked product and gases were observed when nano catalysts were used.

- A prominent cracking of hydrocarbons into "2-ethylpentane, Cyclopentane, cyclohexane, methyl pentane, isopentane, butane,2,2,3-trimethyl, cyclohexanemethane, 2,2-dimethylpentane, and Methyl cyclohexane etc" was observed while cracking under sunlight and uv light.

- Pyrex glass wares were utilized for experiments it has inherent problem of absorption of light in the wavelength range of 320 nm and below that's why no satisfactory results were obtained at UV 254 nm range.

- Photosensitive nano catalysts i.e. TiO_2 and ZnO produce better results as compared to MgO nanopaticles.

6.2. Future Plans

Petroleum field is very demanding so any minute improvement in its refining will be of much greater help to the industry and will help to withstand the speedy depletion of crude resources.

6.2.1. Plant Design

For ultimate success and ultimate quality product, designing a proper plant which caters for the temperature control and safety of catalyst and product is of utmost importance. Successful plant designing will encourage for further research in this very project (relating to petroleum) which has very tough competition and demand ahead. As catalysts used here are of nano size which require a precise design of plant as to prevent any waste of nano catalysts. Moreover, increase in demand of crude resources and speedy depletion of natural reservoirs demands a detailed designing and thought full research on the petroleum field to comply with increasing petroleum demands.

6.2.2. Catalyst's Regeneration

In order to get the maximum output from the least input in regard of both quality and quantity catalyst plays an important role. Petroleum refining started using catalysts in the bulk form which is now on its verge to shift to nano regime keeping its obvious results in view. However, nano catalyst being very fine in its geometry and precious due to its difficult preparation and cost are required to be regenerated after use and prevented from any unwanted wastage.

Bibliography

[1] http://www.bvt.umweltbundesamt.de/archiv-e/lvocbref-e.pdf, acessed on February 29th, 2008.

[2] P. Eisele, Killpack, R., Propene, 4 (2005).

[3] A. Meyers, McGraw-Hill, .Handbook of Petrochemicals Production Processes" Handbooks,, 3rd edition, (2004).

[4] I. Safrik, Strausz, P., Research on Chemical Intermediates,, 22, ((1996)) pp. 275.

[5] L. Starkbaumová, Belohlav, Z., Zámostný, P.,, Primary reactions and products of hydrocarbon pyrolysis, ((2005)).

[6] K. Sundara, Froment G, Modeling of thermal cracking kinetics. 3. , 17 (1978) pp.174.

[7] S. Chaturvedi, P.N. Dave, N.K. Shah, Journal of Saudi Chemical Society, 16 (2012) 307.

[8] A.B. Jatinder Kumar, Materials Science Forum, Vol. 764 (2013) pp 130.

[9] F.H.J. J., Journal of Chemical Society . ,65 (1994) 899.

[10] A. Mills, Davies, R. H., Worsley, D. , Chemical Society Reviews, 22 (1993) 417.

[11] R.W. Matthews, Journal of Catalysis, 111 (1988) 264.

[12] Y. Luo, Handbook of bond dissociation energies in organic compounds, cap. 3, 4, 11 (2003).

[13] A. Mills, Hunte, S. L, Journal of Photochemistry and Photobiology, 108 (1997) 1.

[14] E.R. Carraway, Hoffmann, A. J., Hoffmann, M. R., Environmental Science and Technology, 28 (1994) 786.

[15] L.B. Khalil, Mourad, W. E., Rophael, M. W.,, Applied Catalysis B: Environmental, 17 (1998) 267.

[16] M.A. Fox, Dulay, M. T., Chemical Reviews. 93 (1993) 341.

[17] L.B. Reutergardh, Iangphasuk, M., Chemosphere, 35 (1997) 585.

[18] N.S. Deng, Wu, F., Luo, F., Xiao, M., Chemosphere, 36 (1998.) 3101

[19] N. Ozalp, K. Ibrik, and M. Al-Meer, Energy, 55 (2013) p. 74.

[20] K.K.b. Mehdi Sedighi a, Jafar Towfighi, Fuel, 109 (2013) 432.

[21] S. Seifzadeh Haghighi, M.R. Rahimpour, S. Raeissi, O. Dehghani, Chemical Engineering Journal, 228 (2013) 1158.

[22] Y. Yoshimura, Catalysis Surveys from Japan,, Vol. 4 (2000) 157.

[23] M. Tahir, N.S. Amin, Energy Conversion and Management, 76 (2013) 194.

[24] P.M. Varghese OK, Latempa TJ, Grimes CA, Nano Lett 2009, 9 (2009) 731.

[25] L.Z. Yang L, Energy Convers Manage 2007, 48 (2007) 882.

[26] L. Zhang, P. Li, Z. Gong, X. Li, Journal of Hazardous Materials, 158 (2008) 478.

[27] P.L.a. Lihong Zhang , Zongqiang Gonga, Xuemei Li, Journal of Hazardous Materials (2008), 158 ((2008)) 478.

[28] M.A. Karimi, Int. Nano Letters, Vol. 1 (2011) 43.

[29] X.-K. Wang, C. Wang, W.-L. Guo, J.-G. Wang, Materials Research Bulletin, 46 (2011) 2041.

[30] I.S. F. Nastase, C. Nastase, D., A.M. Mihaiescu, Prog. Solid State Chem. , 34 (2006) 191.

[31] A.B. Sreekanth K. Mahadeva, Nanomaterials 2013, 3(3) (2013) 486.

[32] J.Z.H.Z. J. Zhu, W. Qin, L. Chai, Y. Hu,, Trans. Nonferrous Met. Soc. China 19 (2009) 1578.

[33] J.Z. H. Guo, Z. Lin, Electrochemistry Communications, Vol 10 (2008) 146.

[34] M.A.M. Alavi, Ali, Iran. J. Chem. Chem. Eng., Vol. 30, No. 3, 2011 75.

[35] Y.L. Clemens Burda, NANO LETTERS Vol. 3, No. 8 (2003) 1049.

[36] A.H. Fujishima, K, Nature vol 19 (1972) 238.

[37] S.U.M.A.-S. Khan, M.; Ingler, W. B., Jr., Science Vol 297 (2002) 2243.

[38] Y.X. L. Han, H. Liu, X. Ma, G. Tang, J., Hazard. Mater., 175 (2010) 524.

[39] C.W. Xi-Kui Wang, Wen-Qiang Jianga, Chemical Engineering Journal, Vol 189–190 (2012) 288.